



MONTCLAIR STATE
UNIVERSITY

Montclair State University
**Montclair State University Digital
Commons**

Theses, Dissertations and Culminating Projects

5-2012

Investigation of Autoregulation of ICER and Electrochemical Properties of Tryptophan

Mark DeMilio
Montclair State University

Follow this and additional works at: <https://digitalcommons.montclair.edu/etd>



Part of the [Biology Commons](#), and the [Chemistry Commons](#)

Recommended Citation

DeMilio, Mark, "Investigation of Autoregulation of ICER and Electrochemical Properties of Tryptophan" (2012). *Theses, Dissertations and Culminating Projects*. 815.
<https://digitalcommons.montclair.edu/etd/815>

This Thesis is brought to you for free and open access by Montclair State University Digital Commons. It has been accepted for inclusion in Theses, Dissertations and Culminating Projects by an authorized administrator of Montclair State University Digital Commons. For more information, please contact digitalcommons@montclair.edu.

MONTCLAIR STATE UNIVERSITY

/ INVESTIGATION OF AUTOREGULATION OF ICER AND
ELECTROCHEMICAL PROPERTIES OF TRYPTOPHAN /

by

Mark DeMilio

A Master's Thesis Submitted to the Faculty of
Montclair State University

In Partial Fulfillment of the Requirements
For the Degree of

MASTER OF SCIENCE

May 2012

College of Science and Mathematics

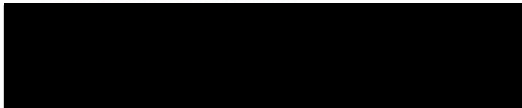
Department of Chemistry & Biochemistry

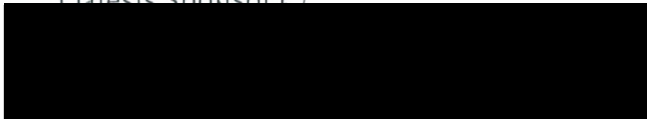
Certified by:


Dr. Robert Prezant
(Dean, College of Science & Mathematics)

May 8, 2012
(Date)

Thesis Committee:


Dr. Johannes Schelvis
(Thesis Sponsor)


Dr. Carlos A. Molina
(Committee Member)


Dr. Shifeng Hou
(Committee Member)


Dr. Marc L. Kasner
(Department Chair)

Abstract

A relatively new development in the field of research-based chemistry is to study biomolecules, their interactions, and a biochemical mechanisms by examination of their physical properties and application of laboratory techniques rooted in concepts of physical chemistry. Both projects that are encompassed within this master's thesis indeed fall under the umbrella of biophysical chemistry, as they apply physical chemical techniques study particular biomolecular interactions.

The first of these two projects is the study of a leucine zipper protein, Inducible cAMP Early Repressor (ICER), which is a product of the cAMP Responsive Element Modulator (CREM) gene. ICER functions as a transcriptional repressor by binding to cAMP Responsive Elements (CRE's) found in the promotor sequences of genes involved in cellular growth, and is abnormally expressed in certain forms of cancer in which ICER acts as a tumor repressor. It also binds to the four CRE sites on its own promotor, known as CARE-1 through CARE-4, thereby regulating its own expression. This research is based on the hypothesis that ICER may in fact autoregulate its own expression by cooperative binding to its own promotor.

A technique known as Fluorescence Resonance Energy Transfer (FRET) is used to test this hypothesis and determine dissociation constants of purified ICER with double stranded DNA. Titrations were performed with purified ICER and double stranded DNA labeled with a fluorophore-quencher pair and containing one or more of the CARE sites. Observed dissociation constants were largely inconsistent and traced back to difficulties in producing purified ICER on a regular basis. Therefore, the focus shifted to reproducible purification of ICER. It includes a comparison of three purification protocols, one of which is a urea-based denaturing purification, another being a native purification, and the third a combination of the first two. Qualitative data that will illustrate this comparison includes side-by-side SDS-PAGE gel electrophoresis analysis of samples from each step of both purification procedures, among other things.

The second project that makes up this thesis involves an enzyme that repairs DNA. The enzyme *E. coli* photolyase utilizes a light-driven electron transfer

mechanism for repairing DNA damaged by UV-light exposure. The enzyme may be activated by a proton-coupled electron transfer (PCET) mechanism. PCET mechanisms are of considerable interest due to their prevalence in many physiological processes such as enzyme catalysis, as they provide an alternative reaction pathway that circumvents traditional high-energy transition states. In this case, during the electron transfer mechanism, the neutral radical form of the flavin adenine dinucleotide cofactor (FADH^\cdot) is reduced to FADH^- , and an amino acid radical intermediate is formed. This amino acid, ^{306}Trp , is of particular significance due to its role in the mechanism.

Using voltammetry, it is possible to measure the reduction potential of the Trp in solution, providing insight into the mechanism involving ^{306}Trp . The ^{306}Trp reduction potential represents the charge recombination energy required for oxidation of that amino acid and formation of FADH^- . As the mechanism of electron transfer involves a proton, its kinetics are heavily pH-dependent. Thus data was acquired over a wide range of pH values in order to quantify this relationship. Furthermore, this reaction was studied in distilled water and in D_2O in order to examine solvent effects on the reduction potential of Trp. An observed "inverse" kinetic isotope is investigated in detail to explain the observed increase in reaction rate in D_2O counterintuitive to the mass-related kinetic isotope effect.

The data from this thesis confirm the hypothesis that D_2O significantly affects the reduction potential and the pKa of Trp, the combined effects of which explain the observed "inverse" isotope effect in which the reaction occurs more quickly in D_2O . All experiments were repeated with a tryptophan-like molecule, N-acetyl-L-tryptophanamide, the properties of which more accurately represent how the ^{306}Trp residue would act in the electron-transfer mechanism as a member of a peptide chain. N-acetyl-L-tryptophanamide, unlike natural amino acids, contains no C-terminus and two amine groups. Therefore, issues of charge formation from amino acid ionization that limited the pH range for the tryptophan experiments were alleviated, and the use of N-acetyl-L-tryptophanamide allowed for greater experimental freedom and lent itself to a wider pH/pD range to be investigated.

INVESTIGATION OF AUTOREGULATION OF ICER AND
ELECTROCHEMICAL PROPERTIES OF TRYPTOPHAN

A THESIS

Submitted in Partial Fulfillment of the Requirements
For the Degree of Master of Science

By

MARK DEMILIO

Montclair State University

Montclair, NJ

2012

Copyright © 2012 by *Mark Daniel DeMilio*. All rights reserved.

Acknowledgements

First and foremost, I wish to thank Dr. Johannes Schelvis, for whom I have the deepest appreciation for giving me the opportunity to work in his lab. His never-ending patience, tutelage, and mentorship have made it an honor to have him as a boss these past few years. Likewise, I would like to thank Dr. Marc Kasner, for his apparently egregious lapse in judgment that led to my hiring as a graduate assistant, and for always keeping my ego in check. Both of you have always been supportive and understanding about my health issues and I never take it for granted.

To Dr. Carlos Molina and Dr. Shifeng Hou, thank you for: your wealth of biochemical and electrochemical knowledge, respectively; your assistance in preparing (and helping me make sense of) various parts of the experimental setups herein; for frequent and sometimes random use of your labs and instrumentation; and donation of chemical supplies as needed.

I would like to thank the faculty of the Department of Chemistry & Biochemistry, all of whom taught me various skills I applied to complete this thesis, as well as the Sokol Institute for their financial contributions to the ICER project. To Franklin Paulino, thank you for your hard work and involvement with the ICER project. Likewise, Agnieszka Zieba, I appreciate your invaluable contribution to the photolyase projects.

To my parents, thank you for keeping me grounded and reminding me how proud they are of me throughout this grueling process despite my physical limitations. To my sister, Julia, I appreciate all of our conversations in the wee hours, which would help get my mind off of yet another late night of work I was putting in towards completing this thesis. All of my colleagues and fellow graduate assistants, I thank you for helping me to stay loose and retain my sanity throughout the completion of this process.

While I'm unable to name every single person who has influenced me or contributed to this project in some form or fashion (and I'm certain to have forgotten some of you), I thank you all nonetheless. I couldn't have done this without each and every one of you.

Table of Contents

	<u>Page</u>
<u>Part One: Investigation of Autoregulation of ICER</u>	
Introduction	5
Materials & Methods	
<i>Expression of ICER</i>	10
<i>Denaturing Purification (pH-based)</i>	11
<i>Native Purification</i>	12
<i>Denaturing Prep Using Imidazole for Purification</i>	13
<i>Determination of Protein Concentration</i>	15
<i>Preparation of Single- and Double-Stranded DNA</i>	16
<i>FRET Analysis of ICER Binding to DNA</i>	18
Results & Discussion	24
Conclusion	31
 <u>Part Two: Electrochemical Properties of Tryptophan</u>	
Introduction	33
Materials & Methods	
<i>Study of Isotope Effects</i>	43
<i>Electrochemistry</i>	45
<i>Cyclic Voltammetry</i>	46
<i>Differential Pulse Voltammetry</i>	47
<i>Redox Standard Couple</i>	47
<i>pH-dependent Study</i>	48
<i>Buffer Solutions</i>	48
<i>Instrumentation</i>	49
Results & Discussion	54
Conclusion	62
 Bibliography	 64

Part One

INVESTIGATION OF AUTOREGULATION OF ICER

Introduction

Inducible cAMP Early Repressor (ICER) is a leucine zipper protein, a product of the cAMP Responsive Element Modulator (CREM) gene, and a known transcription repressor (1). It is abnormally expressed in certain kinds of cancer in which ICER acts as a tumor repressor (2). ICER is involved in the repression of genes activated by the cAMP signaling pathway, doing so by binding to the cAMP Responsive Elements (CRE's) found in the promoter sequences of genes involved in cellular growth. The ICER gene contains four CRE elements, shown in Figure 1, known as CARE-1 through CARE-4 located in its own promoter (2), and repression of the promoter activity and regulation of its own expression involves binding of ICER to one or more of these CRE elements.

Leucine zippers such as ICER exist in solution as homodimers and maintain a parallel coiled-coil motif as shown in Figure 2, where the two flexible DNA-binding strands are bound in a fashion structurally resembling an open pair of scissors (3). As the name suggests, individual strands of these proteins have a periodic array of leucine residues appearing at every seventh position, exist in an alpha-helical conformation, and extending leucine side chains interact with those of a neighboring helix, allowing for dimerization and formation of a coiled coil motif (4). This particular three-dimensional structure is critical to the site-specific recognition of DNA binding sequences, and studies have been performed to examine this binding specificity by incorporating high-affinity binding sites into random-sequence DNA and examining the binding activity (5, 6).

Such studies that have been performed on comparable leucine zipper proteins shown to repress transcriptional activity of genes amplified in many tumors have largely explored binding affinity to particular binding sites in DNA. However, in the presence of multiple binding sites, there exists a possibility for cooperative binding to occur as well. Cooperative binding, as Figure 3 illustrates, is found when a biomolecule's affinity for its ligand increases with the amount of bound ligand; such a mechanism is present in humans, where hemoglobin's tertiary structure changes upon initial oxygen binding to facilitate subsequent binding for other oxygen molecules (7). Mathematical analysis of one-site binding and of cooperative binding is very similar, as shown in Equations 1 and 2 respectively. Both analyses require accurate quantitative data of the same parameters; however, the model for cooperative binding also accounts for—and mathematically contextualizes—the possible effects of having multiple binding sites present (i.e., cooperativity), or a lack thereof.

Due to the current lack of quantitative studies on ICER specifically, it was necessary to create a binding model based on the two-step mechanism proposed in published studies of ICER-like (leucine zipper) proteins (8-13). When similar transcriptional factors with a leucine zipper motif have been analyzed for binding preferences, quantitative analysis has shown the potential existence of several binding models, all of which require precise and quantifiable measurements. These include traditional one-step models for both single and multiple binding sites, as well as multi-step mechanisms containing a pre-equilibrium for both of these scenarios (14). More recent developments have detailed a two-step mechanism in

which the protein dimerizes in the pre-equilibration step and the following step characterizes protein-DNA interactions (β). The results herein were largely analyzed by applying this proposed two-step mechanism shown in Figure 4, in which two dissociation constants arise: K_{d1} , the “pre-equilibrium” step representing the dimerization of the leucine zipper, and K_{d2} , which denotes the binding between the homodimer and DNA.

Binding studies of purified ICER protein and fluorescently tagged DNA containing one or more CARE sites can be performed to study the mechanism of autoregulation of ICER and, to a broader extent, its function and capacity as a transcription repressor and potential tumor antagonist. In doing so, the dissociation constants of ICER and each individual CARE sites could be determined, and studies with DNA containing multiple CARE sites examine the potential for cooperative binding. Thus, analysis of interactions between ICER and DNA containing multiple CARE sites (in comparison to results with a single CARE site) could determine the existence, if any, and potential extent of positive cooperative binding between the different binding sites on the CREM gene promoter.

Quantitative analyses of protein-DNA interactions require the use of highly purified protein, and typically produce dissociation constants on the order of nanomolar, and sometimes much smaller (β). In dealing with such strict parameters, the potential for error and statistical deviation is greatly augmented, and any issues causing poor experimental reproducibility can bring about many problems in generating and replicating worthwhile data. Over the course of this project, there have been recurring issues of ICER sample impurity that have largely contributed to

the lack of reproducible data. As such, the focus has shifted from obtaining as much quantitative insight of ICER-DNA binding interactions as possible, to examining, comparing and assessing the effectiveness of the different methods used to purify ICER. The seemingly reliable data collected and subjected to quantitative analysis, while minimal, will also be discussed in reasonable detail, as well as any other resultant information that may be gleaned from the successes and failures of this project.

5'-CAGT**GAGCTGC**ACATT**GATGGC**GTGAT
AGGCTGG**TGACGTCA**CTGT**GATGTCA**GTGC
TCCTACTTATCTTACATATGCTTGCTAC-3'

Figure 1. CRE elements on the CREM gene promotor sequence. CARE-1 (nine residues in length) and CARE-2 (eight residues) are indicated in darker red, and CARE-3 and CARE-4 (both eight residues) are shown in lighter red. The four CARE sites appear in sequential order starting from the 5' end of the oligonucleotide. The possibility for positive cooperativity exists due to the close proximity of the four binding sites on the promoter (2).

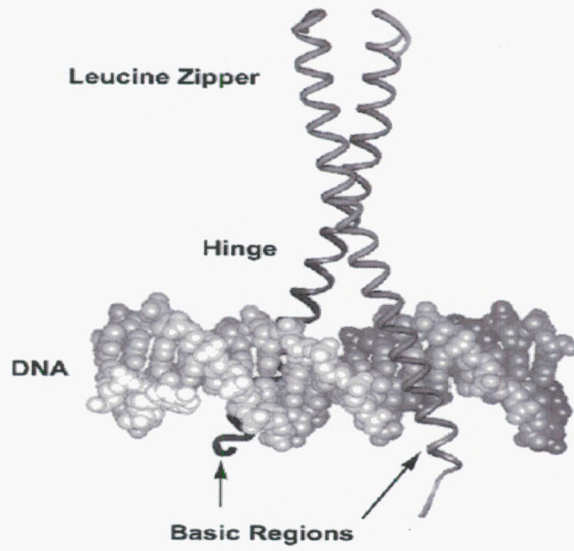


Figure 2. Structural model of a homodimer leucine zipper protein, shown bound to DNA. Hydrophobic leucine zipper region is responsible for dimerization and coiled coil motif; basic regions interact with DNA (10).

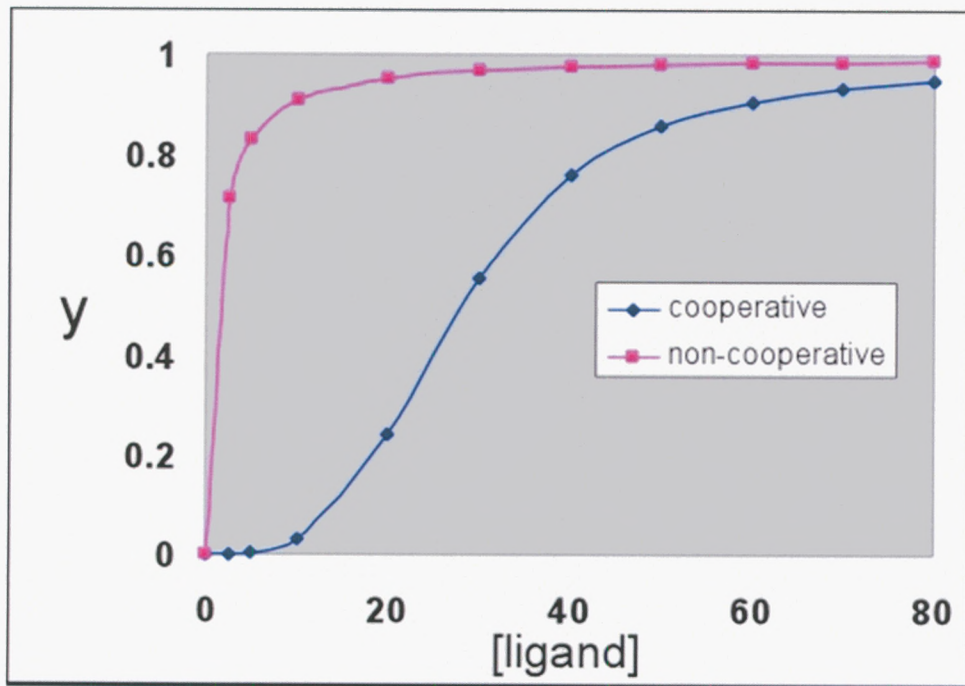


Figure 3. Generic model of cooperative and non-cooperative binding curves. Cooperative binding curves follow a sigmoidal pattern, demonstrating that amount of bound ligand increases with the amount of ligand already bound, whereas non-cooperative models display a typical hyperbolic binding curve. (J.D. Cronk. Lecture 16. The allosteric properties of hemoglobin. <http://guweb2.gonzaga.edu/faculty/cronk/CHEM440pub/L16-index.cfm> (accessed 3/30/12).)

$$Y = \frac{[ICER]}{K_d + [ICER]}$$

Equation 1. One-site binding model, demonstrating the mathematical relationship between ICER concentration and observed dissociation constant. General basis comes from Hill equation. (Hill, A.V. *J. Physiol.* **1910**, *40*, 4-8)

$$Y = \frac{[ICER]^n}{K_d^n + [ICER]^n}$$

Equation 2. Multiple-site binding model accounting for possible binding cooperativity. Extremely similar to Equation 1, uses the same numerical parameters, but also takes into account the possibility of cooperative binding in the form of the cooperativity number, n , also known as Hill coefficient. (Hill, A.V. *J. Physiol.* **1910**, *40*, 4-8)

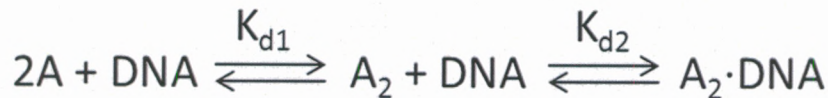


Figure 4. Proposed mechanism for formation of ICER (A) homodimer-DNA complex. K_{d1} is the “pre-equilibrium step” of ICER dimerization, while K_{d2} is the equilibrium constant for protein-DNA binding (8).

Materials & Methods

Expression of ICER. ICER was expressed *in vitro* with a 6xHistidine tag on the N-terminus in cell cultures of BL21DE3 bacteria (2). An LB broth (10.0 g/L bacto-tryptone, 5.0 g/L bacto yeast extract, 5.0 g/L NaCl) was inoculated with an *E. coli* colony harboring the necessary expression vector and grown at 37°C overnight. The overnight culture is diluted 1:60 with fresh LB medium containing antibiotics used to eliminate all constituents of the expression system save for 6xHis-tagged ICER from growing, and subsequently grown while shaking at 37°C until the absorbance of the solution at 600 nm reached 0.6. After this, IPTG was added to a final concentration of 1.0 mM, in order to induce overexpression of the ICER gene, and

the culture was shaken at 37°C for 4 hours. The broth was divided into 5.0 mL aliquots in centrifuge tubes, which were spun down at 4000 $\times g$ for 15 minutes to harvest cells. Cells were then stored at -80°C until purification.

Denaturing Purification (pH-based). Each individual pellet was thawed for 15 minutes and resuspended in 700 mL of Lysis Buffer B (7.0 M urea, 0.1 M NaH₂PO₄, 0.01 M Tris-Cl, pH 8.0). The cell lysate was homogenized and redistributed in 700 μ L aliquots. After 15 minutes, 15 units of Benzonase Nuclease (25.0 units/mL) were added and the cells were incubated with agitation for 15 minutes at room temperature, and, if necessary, vortexed until lysis was complete (solution becomes milky and translucent, with no solid bits left, once lysis has fully finished). Cell lysate was centrifuged at 12,000 $\times g$ for 25 minutes at room temperature in order to pellet the cellular debris, and the supernatant was collected (a 50 μ L aliquot of each sample of cleared lysate was saved for future SDS-PAGE analysis). One Ni-NTA spin column (Qiagen) was equilibrated for each pellet with 600 μ L Buffer B, and centrifuged with an open lid for 2 minutes at 890 $\times g$. 600 μ L of cleared lysate supernatant was added to each pre-equilibrated Ni-NTA spin column, and centrifuged 5 min at 270 $\times g$, and the flow-through was collected. Each column was washed with 600 μ L Wash Buffer C (7.0 M urea, 0.1 M NaH₂PO₄, 0.01 M Tris-Cl, pH 6.3) three consecutive times to clean the cell lysate, leaving only the 6xHis-tagged ICER bound to the positively-charged nickel column. The protein was then eluted twice with 200 μ L Elution Buffer E (8.0 M urea, 0.1 M NaH₂PO₄, 0.01 M Tris-Cl, pH 4.5), yielding a total of 400 μ L purified protein. The protein solutions were then rid of urea using 3 kDa filter columns using Wash Buffer B containing no urea in several

dilution steps. An initial tenfold dilution was performed prior to filtration, and subsequent spin cycles to allow for additional tenfold dilution were then performed to assure that the final urea concentration in solution was less than 1.0 mM. Previous control experiments in which solutions containing only 10.0 mM, 1.0 mM, and 0.1 mM urea were titrated into dsDNA strands to check for any effect of the molecule's presence on binding experiments showed that a resultant urea concentration of <10.0 mM did not have any impact and was sufficiently low for any titrations with ICER solutions and dsDNA.

Once urea removal was complete, the overall protein concentration of each sample was determined via BCA Assay, using bovine serum albumin (BSA) as an external standard, and myoglobin as a control. (Note: ICER does not absorb in the visible spectrum; as such, it is not possible to simply determine ICER concentration in the protein solutions. Instead, only total protein concentration may be determined – therefore the purity of each protein solution is critical to establishing an accurate quantitative picture of the concentration of ICER.)

Native Purification. Pellets were thawed at room temperature for 15 minutes, and resuspended in 700 μ L of Lysis Buffer B, 20 mM imidazole (0.1 M NaH_2PO_4 , 0.01 M Tris-Cl, 20 mM imidazole, pH 8.0), vortexed as necessary to ensure complete lysis. The cell lysate was homogenized and redistributed in 700 μ L aliquots. 100 μ L of 10.0 mg/mL lysozyme (provided by Dr. Dyer, Department of Chemistry & Biochemistry at Montclair State University) was added to the solution containing the resuspended cells, and the solution was stored at 4°C for 30 minutes while Ni-NTA columns were pre-equilibrated with Lysis Buffer B, with 20 mM

imidazole instead of 7.0 M urea, in the same fashion as in the denaturing purification. After the incubation period, cells were submerged in water and sonicated for 4 minutes, and 1.0 mL of 25 units/mL Benzonase Nuclease was added afterwards. Cell lysate was centrifuged at $12,000 \times g$ for 25 minutes at room temperature in order to pellet the cellular debris, and the supernatant was collected (a 50 μ L aliquot of each sample of cleared lysate was saved for future SDS-PAGE analysis).

After centrifugation, 600 μ L of cleared lysate was added to each column and bound by spinning at 1,500 RPM for 5 minutes (flow-through was collected for further analysis). The columns were washed three times as in the denaturing prep, using Wash Buffer C, 60 mM imidazole instead of 8.0 M urea (0.1 M NaH_2PO_4 , 0.01 M Tris-Cl, 60 mM imidazole, pH 8.0), and eluted twice, using 200 μ L of Elution Buffer E, 500 mM imidazole instead of 8.0 M urea (0.1 M NaH_2PO_4 , 0.01 M Tris-Cl, 500 mM imidazole, pH 8.0), in each individual step. A total of 400 μ L of purified protein was collected for each column. Imidazole was then removed using 3 kDa filter columns using Buffer B with no imidazole or urea. Total protein concentration was then determined via BCA Assay, with BSA as a standard, and a myoglobin control.

Denaturing Prep Using Imidazole for Purification. As issues of purity and poor sample reproducibility arose in using the two abovementioned purification techniques, a combination of the techniques was applied in which each of the buffers contained varying concentrations of imidazole in addition to a high concentration of urea. Likewise, the pH of all buffer solutions was kept at 8.0 throughout the procedure. Pellets were thawed at room temperature for 15

minutes, and resuspended in 700 μL of Lysis Buffer B, 20 mM imidazole (0.1 M NaH_2PO_4 , 0.01 M Tris-Cl, 20 mM imidazole, 7.0 M urea, pH 8.0), then vortexed as necessary to ensure complete lysis. After 15 minutes, 15 units of Benzonase Nuclease (3.0 units/mL) were added, the cells were incubated with agitation for 15 minutes at room temperature, and, if necessary, vortexed until lysis was complete.

Cell lysate was centrifuged at 12,000 $\times g$ for 25 minutes at room temperature in order to pellet the cellular debris, and the supernatant was collected (a 50 μL aliquot of each sample of cleared lysate was saved for future SDS-PAGE analysis). One Ni-NTA spin column was equilibrated for each pellet with 600 μL Buffer B, and centrifuged with an open lid for 2 minutes at 890 $\times g$. 600 μL of cleared lysate supernatant was added to each pre-equilibrated Ni-NTA spin column, and centrifuged 5 min at 270 $\times g$, and the flow-through was collected. Each column was washed with 600 μL Wash Buffer C, 60 mM imidazole (7.0 M urea, 0.1 M NaH_2PO_4 , 0.01 M Tris-Cl, 60 mM imidazole, 8.0 M urea, pH 8.0) three consecutive times to clean the cell lysate, leaving only the 6xHis-tagged ICER bound to the positively-charged nickel column. The protein was then eluted twice with 200 μL Elution Buffer E, 500 mM imidazole (0.1 M NaH_2PO_4 , 0.01 M Tris-Cl, 500 mM imidazole, 8.0 M urea, pH 8.0), yielding a total of 400 μL purified protein from each column. The protein solutions were then rid of urea using 3 kDa filter columns using Wash Buffer B containing no urea. Once urea removal was complete, the overall protein concentration of each sample was determined via BCA Assay, using bovine serum albumin (BSA) as an external standard, and myoglobin as a control.

Determination of Protein Concentration. As mentioned earlier, ICER does not absorb in the visible spectrum; as such, it is not possible to simply determine ICER concentration alone in the protein solutions by applying Beer's Law. Instead, only total protein concentration may be determined – therefore the purity of each protein solution is critical to establishing an accurate quantitative picture of the concentration of ICER. The bicinchoninic acid (BCA) Assay is a relatively simple and extremely common biochemical technique used to determine concentration of protein in solution, which works under alkaline conditions. The technique, using a sodium salt of BCA, monitors the formation of cuprous ion produced in the reaction of protein with Cu^{2+} by color change (15) It has been demonstrated that certain amino acid residues such as cysteine and tyrosine, and peptide bonds, are able to form a complex with Cu^{2+} and subsequently reduce the copper ions to Cu^+ (16). BCA in turn forms a purple complex with Cu^+ in alkaline solution, and measuring the absorbance of the solution at 562 nm makes it possible to quantify the reduction of Cu^{2+} by proteins present (17).

Stock solutions for each assay were prepared fresh for each time by mixing BCA solution ordered from Sigma-Aldrich, at a 50:1 volumetric ratio with $\text{Cu(II)SO}_4 \cdot 5\text{H}_2\text{O}$ solution. Two blanks were made using 1.0 mL of stock solution and no protein. Standards were prepared containing, respectively, 5, 15, 25, 35, and 45 μg of BSA, along with a control sample with 25 μg of myoglobin. Samples containing 100 μL purified ICER were prepared containing 50 μL of the original ICER solution diluted 1:1 with distilled water, and all protein samples were given the necessary

amount of stock solution to create a total volume of 1.0 mL, incubated for 30 minutes at 60° C and cooled.

A standard curve as shown in Figure 5 was prepared using the five BSA standards and the myoglobin control was used to further verify the quality of the results. From these numbers, the concentration of total protein in the diluted ICER samples could be determined, and application of the dilution factor revealed the working concentration of ICER in purified samples. While this value did represent the total protein concentration and not simply that of ICER, if the samples were shown to be sufficiently pure by SDS-PAGE analysis, these concentrations were used in future quantitative ICER-dsDNA binding studies.

Preparation of Single- and Double-Stranded DNA. Dry oligonucleotide samples of various strains of single-stranded DNA containing one or more CARE sites were purchased from Eurofins MWG – Operon (Huntsville, Alabama). Each DNA sample was labeled with a 6-FAM fluorophore at the 5'-end and with a BHQ1 quencher at the 3'-end. Oligonucleotides varied in length from 20-44 base pairs, and were divided into two categories: "complementary", strands that do not absorb in the visible spectrum, and "fluorescent", or "probe", strands that do absorb in the visible spectrum. Each particular classification of dsDNA (e.g., CARE-1, 21 bp) contained one complementary strand of full length (21 bp, in this example) and one probe strand containing one less residue (20 bp, in this case). When prepared for use, the oligonucleotides were suspended in 0.1 M NaH₂PO₄, 0.01 M Tris-Cl buffer solution, pH 8.0, and stored at -80° C when not in use. Each complementary DNA sample was diluted to 1.3 μM, and probe strands diluted to 1.0 μM. The information

sheet accompanying each shipment of oligonucleotides provided the necessary dilution factor for each strand required to yield 100 mM DNA, as well as its extinction coefficient. UV-vis spectroscopy (Perkin-Elmer P40) was used to monitor the accompanying dilution to 1.0 mM and confirm the concentration as such with Beer's Law and the provided extinction coefficient.

Preparation of double-stranded DNA of each classification required mixing its two strands to allow annealing at an equal ratio. First, 800 μL of 0.5 μM probe strand was prepared by performing a 1:1 dilution with 0.1 M NaH_2PO_4 , 0.01 M Tris-Cl buffer solution, pH 8.0. This solution was titrated with 400 μL of 1.3 μM complementary strand, equating to a 10% excess of a perfect ratio, in 10 aliquots of 40 μL , for a total volume of 1200 μL . In between delivery of an aliquot and taking a reading, the solution was stirred for 10 seconds and allowed to sit for two minutes and thirty seconds to properly allow for mixing and binding to occur between strands. Due to the sensitivity and extremely small numerical scale of the measurements in these experiments, it was imperative to make certain that 100% of the fluorescent strand in solution was bound to its complement, and adding the complementary strand in 10% excess assured that there would be no single-stranded fluorescent DNA left in solution after the titration. This ensured that all fluorescent DNA would bind to its complement, halving the concentrations of each to 0.5 μM . Between this and applying the 2/3 dilution factor following titration of the complementary strand, the resultant dsDNA solution is acknowledged to be 0.33 μM . Excess complementary single-stranded DNA in the solution is innocuous in that it does not absorb in the visible spectrum, but fluorescent DNA that is not bound

would have an effect on subsequent measurements of ICER-DNA binding that also required a fluorometer, and more importantly, it then wouldn't even be possible to accurately determine the concentration of dsDNA in solution as a result.

Due to the presence of the fluorophore and quencher molecules on the oligonucleotide strands, a phenomenon known as Förster Resonance Energy Transfer or Fluorescence Resonance Energy Transfer (FRET) takes place in solution, which allows annealing of the strands to be monitored by fluorescence spectroscopy on the Cary 300 Fluorometer: the initial probe strand solution had a small fluorescence intensity at 520 nm, and as each aliquot of complementary strand was added, the fluorescence signal would increase. Thus, annealing of the two strands could be indirectly confirmed by an observed increase in fluorescence intensity of the solution at 520 nm. Duplicate readings were taken at each step of the titration, and then averaged for quantitative analysis. Settings for the Cary 300 instrument were as follows: excitation λ : 485 nm; emission λ : 505-560 nm; excitation slit: 10 nm; emission slit: 5 nm. A successful annealing process would display itself as an observed increase in fluorescence intensity after each addition of complementary strand solution similar to Figure 6, and an overall increase that typically was around four-fold, and since the complementary strand was added in excess, it could be reasonably stated that annealing occurs to completion.

FRET Analysis of ICER Binding to DNA. Förster Resonance Energy Transfer (FRET) Analysis is an analytical method that has become more prevalent in biochemistry research over the last few decades due to its enormous utility, high sensitivity, non-corrosive and non-invasive nature, and comparative simplicity as a

technique for studying receptor/ligand interactions and geometrical characteristics of small structures containing two chromophores like that shown in Figure 7. FRET is the physical phenomenon by which energy transferred non-radiatively from an excited donor molecule, i.e. the fluorophore, to the acceptor molecule, or quencher, by means of intermolecular long-range dipole-dipole coupling; essential requirements for effective transfer are adequate overlap of the fluorophore's emission spectrum and the quencher's absorption spectrum as displayed in Figure 8, acceptable distance between chromophores (10 to 100 angstroms), parallel (or near-parallel) orientation of transition dipoles of the fluorophores, and sufficiently high quantum yield and absorption coefficient of the fluorophore and quencher molecules, respectively (18). FRET analysis monitors this phenomenon by first exciting the donor molecule, then measuring the fluorescence intensity of the solution of interest at a wavelength suitably applicable to the necessary conditions of overlap between the donor fluorescence spectrum and acceptor absorbance spectrum (in the case of these experiments, this wavelength was 520 nm).

The rate of dipole-dipole energy transfer and intensity of observed fluorescence as shown in Equations 3-5 is, keeping all other aforementioned parameters equal, largely based on the distance between the two chromophores. More specifically, an inverse sixth powers distance dependence of energy transfer was originally experimentally confirmed in the 1960's (19) and has been accepted ever since. Hence, energy transfer from the donor molecule to its acceptor is at its lowest when they are farthest apart, and increases as the two chromophores are brought closer together, resulting in a decrease in fluorescence intensity from the

donor molecule (20). Prior studies of interactions between leucine zippers and double-stranded DNA have shown that, as the protein binds, the DNA strands react accordingly by “bending” inwards, bringing the N- and C-termini closer to each other (10, 21). As increasing amounts of protein are bound, this “bending” does increase proportionally, and the DNA ostensibly starts to form a U-shape as a result as depicted in Figure 9. This change in shape resulting from protein binding can be monitored by fluorescence spectroscopy, allowing for quantifying binding analysis when the resultant data is applied to the suitable binding model. Indeed as this change in the complex’s geometry provides an excellent template for FRET analysis, and all DNA samples containing the CARE sites were labeled with a fluorophore molecule and quencher molecule at opposite ends for this express purpose.

Once a pair of purified ICER and dsDNA samples was chosen for binding studies, an experimental system similar to that of dsDNA formation was set up to monitor the binding via FRET analysis. A 400 μL aliquot of purified ICER solution was diluted in buffer to a concentration of 2.0 μM , in which the requisite dilution factor was based on the protein concentration in the solution initially determined via BCA Assay. Then, a 600 μL aliquot of dsDNA was prepared to a concentration of 0.05 μM by adding 91 μL of the 0.33 μM dsDNA solution to 509 μL of buffer. This ICER-DNA concentration ratio was chosen to ensure that there would be forty times as much ICER in solution as DNA by the end of the titration. The diluted dsDNA solution was placed in a quartz cuvette, and the cuvette was cleaned using a Kimwipe to remove any dust or fingerprints before being placed into a Cary 300 fluorometer. An initial fluorescence intensity reading was recorded in duplicate.

Much like the procedure outlined above, the 400 μL of 2.0 μM ICER solution was titrated into the dsDNA solution in 20 μL aliquots, for a total of 20 aliquots, with duplicate measurements following each addition, and 42 fluorescence intensity readings at 520 nm in total for each titration. Readings were taken in duplicate to be averaged for reducing error in quantitative analysis. The instrument settings were the same as above (excitation λ : 485 nm; emission λ : 505-560 nm; excitation slit: 10 nm; emission slit: 5 nm).

When no ICER is bound to the DNA, the strands are completely straight and the fluorophore is at a maximum distance from the quencher, therefore the initial fluorescence of the solution is at its highest possible intensity. From here, if the titration is successful, the fluorescence intensity will decrease over the course of the titration—that is, more so than the effect that dilution would have on that value—and indicates that ICER has bound to the dsDNA at significant enough quantity as to “bend” the DNA in on itself, bringing the 6-FAM fluorophore and acceptor molecule closer together. Graphically depicting a scatter plot of the average fluorescence intensity of solution at 520 nm as a function of protein concentration in solution will demonstrate the effectiveness of ligand/receptor binding for that particular titration from a visual standpoint without necessitating any further mathematical alterations or corrections. For large-scale analysis of a promising titration, which demonstrates a significant interaction between ICER and DNA based on graphical analysis of the raw data, certain equations are then used and changes and correction factors must be applied to the data.

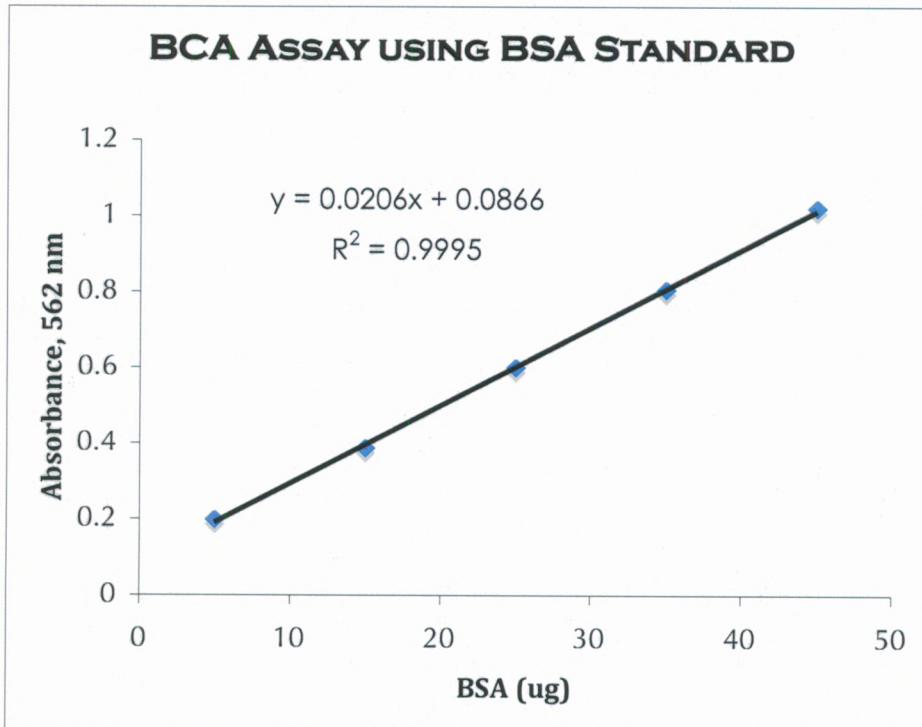


Figure 5. BCA Protein Assay Standard Curve. Bovine Serum Albumin (BSA) is used as the external protein standard. Inset: linear regression analysis for determination of ICER samples of unknown total protein concentration.

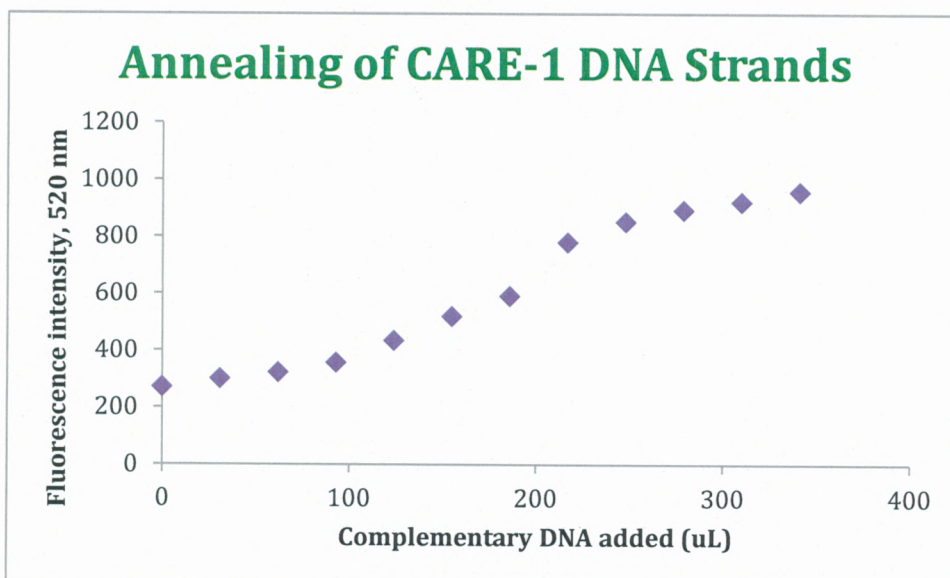


Figure 6. DS DNA annealing curve for oligonucleotides containing only the CARE-1 binding site. Observed increase in fluorescence intensity as larger amounts of 20-bp, single-stranded “complementary” DNA are titrated into the solution containing the 21-bp partner single-stranded “fluorescent” DNA indicates annealing and thus formation of double-stranded CARE-1 DNA, 21 bp, to be used for ICER binding studies.

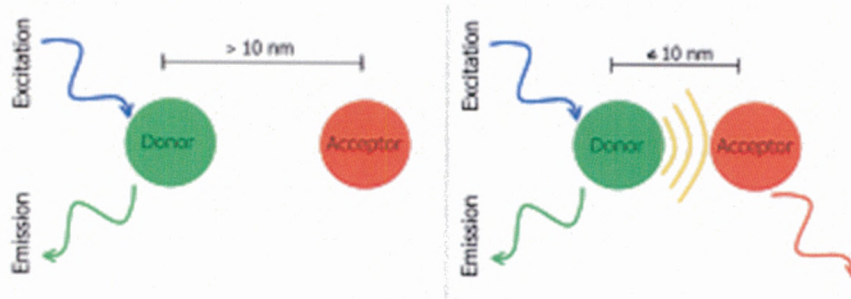


Figure 7. Illustration of non-radiative transfer of photon energy from an excited donor fluorophore to an acceptor fluorophore, i.e. FRET. As depicted, the energy transfer does not occur unless the two chromophores are within the close enough proximity of 10 nm or less [20].

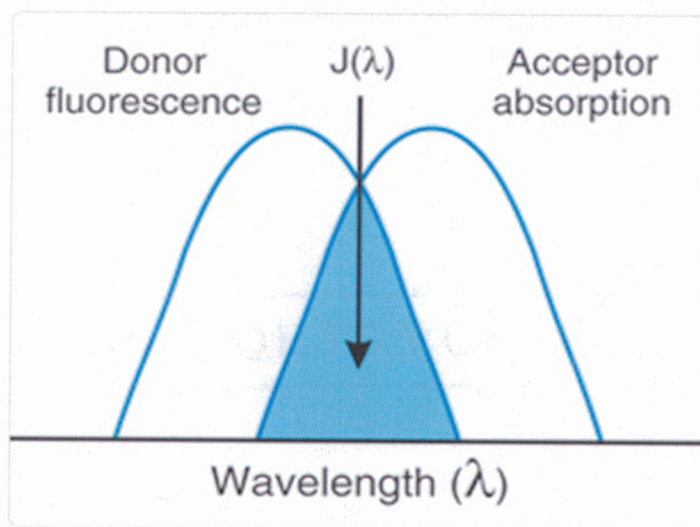


Figure 8. Spectral overlap required for FRET to occur. $J(\lambda)$ represents the midpoint wavelength of overlap, and the optimal wavelength for subsequent fluorescence intensity measurements for FRET analysis. (Invitrogen. Fluorescence Resonance Energy Transfer. <http://www.invitrogen.com/site/us/en/home/References/Molecular-Probes-The-Handbook/Technical-Notes-and-Product-Highlights/Fluorescence-Resonance-Energy-Transfer-FRET.html> (accessed 4/7/12).)

$$k_T = \frac{1}{\tau_D} \left(\frac{R_0}{R_{DA}} \right)$$

Equation 3. Rate of energy transfer of FRET demonstrating inverse dependence (18).

$$R_0 = \sqrt[6]{\frac{\kappa^2}{n^4} \int F_D(\nu) \epsilon_A(\nu) \nu^{-4} d\nu}$$

Equation 4. Förster distance of fluorophore and quencher (18).

$$Q.F. = \frac{R_{DA}^6}{R_{DA}^6 + R_0^6} \tau_D k_F$$

Equation 5. Quantum yield of fluorescence from FRET as determined by parameters in Eq. 3-4 (18).

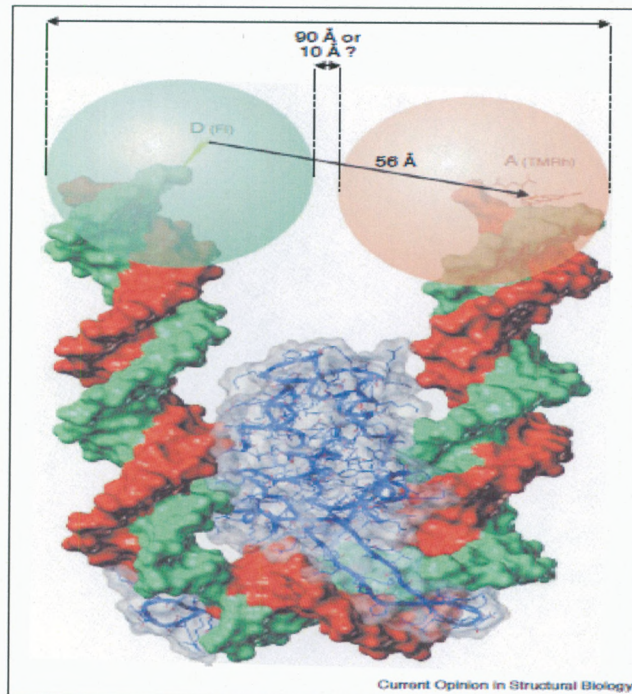


Figure 9. Cartoon depicting FRET in a protein-DNA complex. Bound protein causes the U-shaped folding of DNA, bringing the two chromophores located on the termini closer together. (Hillish, A.; Lorenz, M.; Diekmann, S. *Curr. Op. Struc. Biol.* **2001**, 11, 201-207)

Results & Discussion

As mentioned previously, the vast majority of titrations proved to be unsuccessful both in terms of reproducibility as well as providing a clear indication of ICER binding (or lack thereof). Only a select few titrations were chosen for further analysis if they showed a consistent and considerable decrease in fluorescence intensity concomitant with the addition of ICER. In order to quantitatively analyze

the results of ICER-dsDNA titrations that showed promise, the raw data was placed into a fit equation as described below. Only a handful of these titrations were put to analysis for determination of dissociation constants: titrations of ICER to a 36 bp strand containing just the CARE-1 site, and titrations of ICER to a 21 bp strand containing just the CARE-2 site. The ICER samples used in these titrations was purified using the original denaturing purification protocol as previously outlined. In other words, only single-site binding analysis was applied due to the lack of reproducibility of titrations involving DNA containing multiple binding sites, and therefore it was not possible to study the possibility of cooperative binding given the limitations encountered during the course of the experiments.

In all seemingly reasonable titrations, the two-step mechanism in Figure 4 was used as the framework for subsequent binding studies. Similarly, the change in fluorescence intensity as a result of ICER binding to DNA was analyzed using Equation 6, a single-binding site fit equation, provided by Jung et al (8), that allowed for the determination of dissociation constants for the one-site binding model with a monomer-dimer pre-equilibrium step, providing a basis of comparison to a similar mechanism as detailed in Table 1. Origin 7.0 software (Origin Lab) was used to create the fit equation and process the raw data accordingly, as well as for creating a graph of the composite results from ICER binding to CARE-1 and CARE-2, respectively, shown in Figure 10. The data acquired of purified ICER binding to strands containing either CARE-1 and CARE 2 as detailed in Table 1, below, yielded binding constants that were of a similar order in magnitude as those in studies by Jung et al on Max85 (8), a leucine zipper protein; however, while the accuracy is

relatively promising, the irreproducibility of those results point towards certain inconsistencies in the overall process, namely the process of purifying ICER from whole cell extract. If any information can be gleaned from the quantitative analysis of these titrations, it is as follows: indeed, the determined dissociation constants of both the CARE-1 and CARE-2 DNA strands are within reasonable range, and on the same order of the results from Jung et al; also, as the values for K_{d1} are smaller than those of K_{d2} by approximately a factor of one thousand, it can be inferred that the binding of ICER to CARE sites may actually be restricted by the ICER dimerization step, and that pre-equilibrium step may be a more important regulatory step than the actual binding of ICER homodimer to the DNA.

From here onward the focus shifted to qualitative analysis of the purification methods as outlined above. Side-by-side SDS-PAGE analysis of the different procedures shown in Figure 11 indicates that while the native purification procedure seems to clean up the protein sample much better, thereby producing an ICER sample of very high purity shown in Figure 11 on right, Lane 7, the total yield of this purified protein is shown to be very small via BCA Assay, and thus inconvenient due to the large amount of protein that is required for FRET analysis. Indeed, titrations using purified ICER samples from native purification were largely unsuccessful and extremely inconvenient to perform due to the relative lack of ICER remaining following purification.

On the other hand, the denaturing purification protocol produces an extremely high yield of ICER, as evidenced by the extremely large band shown at its molecular weight in Figure 11 on left, Lane 7. However, this method fails to remove

other protein efficiently during purification of the whole cell extract. Therefore, when the concentration of eluent from the denaturing protocol is determined via BCA Assay, it is not a reasonable estimate of ICER concentration at all and includes all of the other protein products that were not washed off during purification, which resulted in an overestimation of the ICER concentration. These complications introduce a degree of variability in the results of calculated dissociation constants, which again are extremely small, and rely on accurate determination of ICER concentration in solution.

Unfortunately, this same trend was seen when the purification protocol combining urea and imidazole was performed as well, and the SDS-PAGE analysis shown in Figure 12 confirmed as such. The observed value of protein concentration of the eluent as determined via BCA Assay was again larger than the true concentration of ICER, to an unknown degree. Hence, when titrations were performed with 26 bp dsDNA containing CARE-3 only, and purified ICER ostensibly at the necessary concentration, little to no binding was observed. To illustrate this point to a rather blunt degree, a final titration was then performed using the same oligonucleotide, but instead of using 2.0 μM protein solution (and thus some undetermined, smaller concentration of ICER), the eluent was only diluted from a stock concentration of 14.35 μM to 10.0 μM and used for the titration.

Again, the purpose of this was to demonstrate (rather crudely) that if there is indeed a significant enough amount of ICER present in solution, it would bind to the DNA accordingly. Using this more concentrated eluent for that titration did cause a significant decrease in fluorescence intensity resulting from ICER binding to the

CARE-3 site to some degree, as Figure 13a demonstrates. The titration was then duplicated, shown in Figure 13b, to further confirm the presence of this ICER binding. Of course, this process only served to provide a qualitative confirmation of this protein-DNA interaction, but it provides a possible starting point for future experiments in which this modified purification protocol is used. Due to the reproducibility of the results shown in Figures 13a and 13b, this modified protocol does show some potential for a more successful method of ICER purification if studied in further detail.

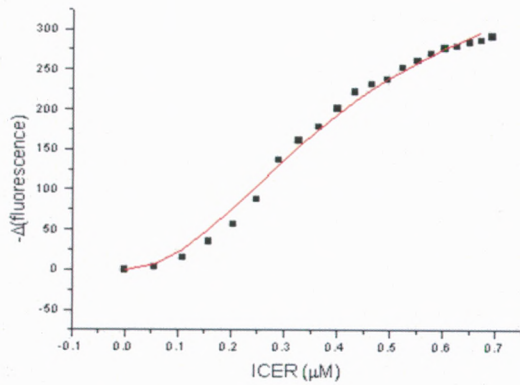
$$I = M \frac{\left(K_{d1} + 4[A]_0 - \sqrt{(K_{d1} + 4[A]_0)^2 - 16[A]_0^2} \right) / 8}{\left(K_{d1} + 4[A]_0 - \sqrt{(K_{d1} + 4[A]_0)^2 - 16[A]_0^2} \right) / 8 + K_{d2}}$$

Equation 6. Applied fit equation for *Origin Binding Analysis* and determination of dissociation constants. $[A]_0$ is the total concentration of ICER in solution. This is the pre-equilibrium model for one binding site as detailed in *Jung et al.*(8). Each titration point was subjected to this analysis.

	CARE 1 (36 bp)	CARE 2 (21 bp)	Jung et al.
K_{d1} (M)	$14 \pm 6 \cdot 10^{-6}$	$17 \pm 5 \cdot 10^{-6}$	$5.9 \pm 0.5 \cdot 10^{-7}$
K_{d2} (M)	$9.6 \pm 0.7 \cdot 10^{-9}$	$2.6 \pm 0.8 \cdot 10^{-9}$	$1.3 \pm 0.2 \cdot 10^{-9}$
K_p (M ²)	$1.3 \pm 0.5 \cdot 10^{-13}$	$4.4 \pm 1.3 \cdot 10^{-14}$	$7.8 \pm 0.5 \cdot 10^{-16}$

Table 1. Dissociation constants for ICER binding to CARE-1 and CARE-2, compared to a paper involving a similar mechanism. K_{d1} represents the monomer-dimer pre-equilibrium step; K_{d2} represents the equilibrium between protein dimer and DNA, and K_p is the product of the two, as outlined in Equation 2. Data on Max85/Max85/DNA dissociation constants (8).

CARE 1



CARE 2

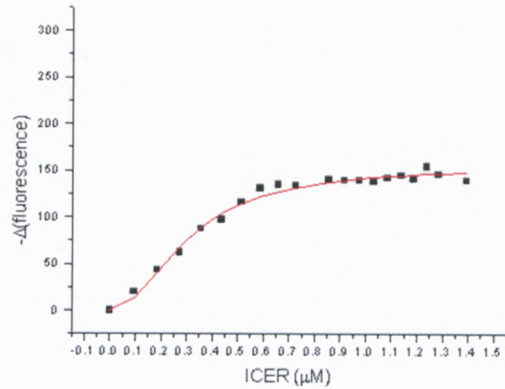


Figure 10. Representative fluorescence intensity changes for binding of ICER to CARE-1 (36 bp) and CARE-2 (21 bp), as depicted by *Origin Binding Analysis*. After applying the fit function shown in Equation 4 to the raw data, the negative change in fluorescence was then used for graphing. This was in order to calculate dissociation constants as per *Jung et al* (8), and accounts for the positive slopes of the graphs that appear counterintuitive to previously detailed principles of FRET as it relates to these experiments.

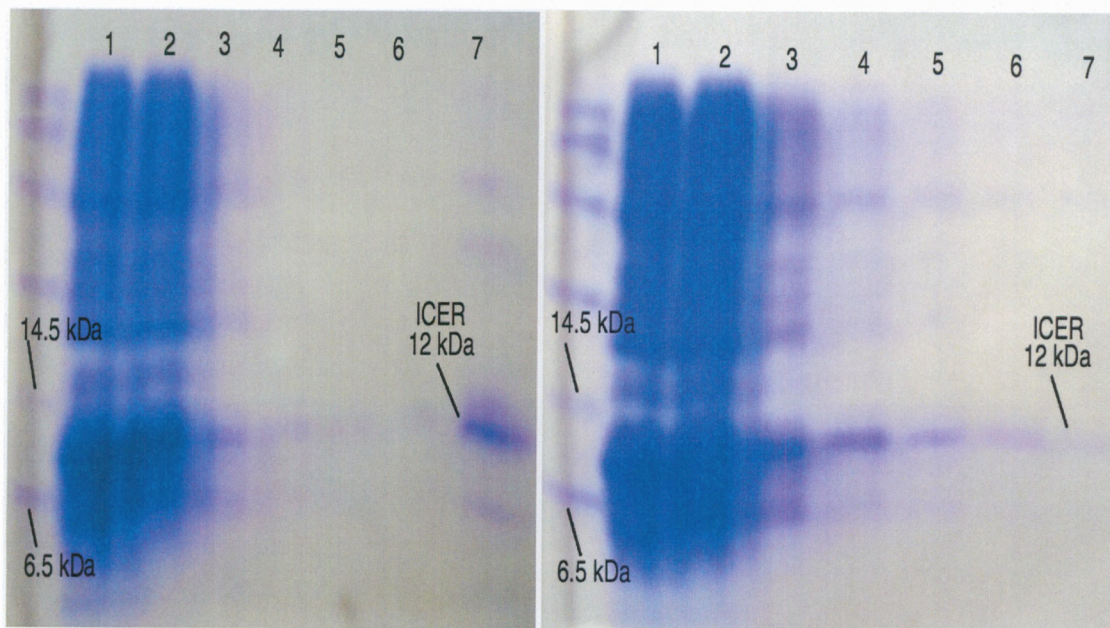


Figure 11. Side-by-side SDS-PAGE analysis of pH-based denaturing purification (left) and native, imidazole-based purification (right) protocols, respectively. Lane 1 is whole cell extract; Lane 2 is flow-through after binding to nickel columns; Lanes 3-6 are successive wash steps; Lane 7 is purified eluate containing ICER.

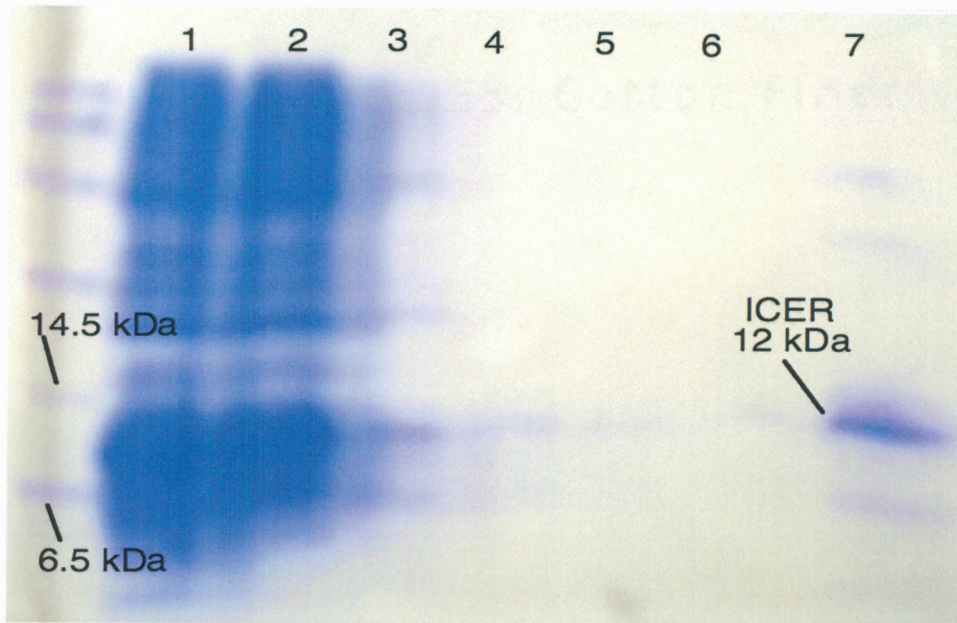


Figure 12. SDS-PAGE analysis of modified purification method using both urea and imidazole. Method fails to rid the protein solution of impurities of both high and low molecular weights, extremely similar to the observed results from the original denaturing protocol.

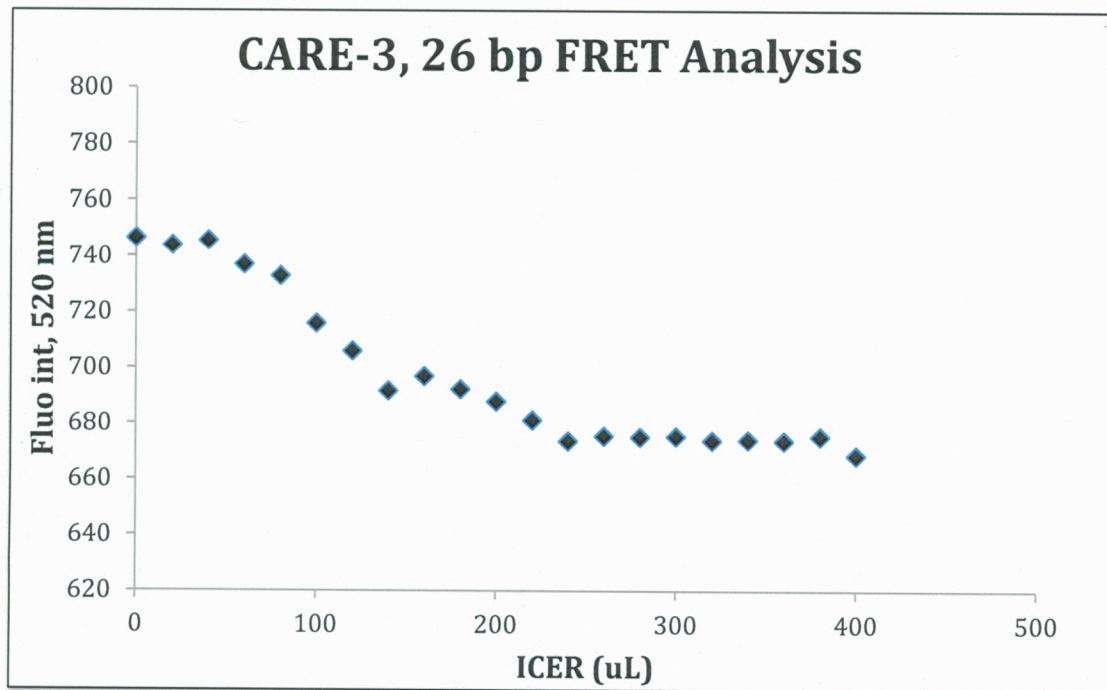


Figure 13a. Excel graphical analysis of duplicate measurements using concentrated eluate, 10.0 mM. Binding clearly occurs between eluate and CARE-3 26 bp when significant excess of ICER solution is used.

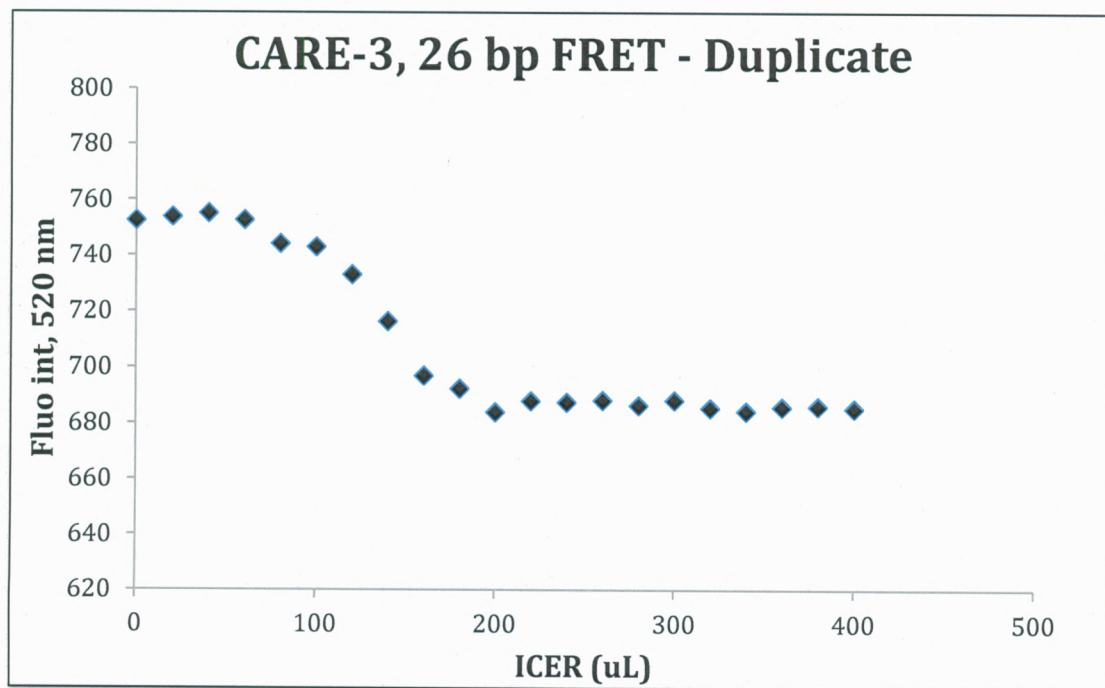


Figure 13b. Excel graphical analysis of duplicate measurements using concentrated eluate, 10.0 mM. Binding clearly occurs between eluate and CARE-3 26 bp when significant excess of ICER solution is used.

Conclusion

Proposed binding models between leucine zippers such as ICER and DNA binding sites can be discriminated and tested by determination of the dissociation constants that are in the micromolar and nanomolar range. However, ICER does not absorb in the visible spectrum, hence colorimetric techniques are largely inapplicable for such quantitative analysis. Due to this, as well as the high sensitivity and susceptibility to deviations of FRET analysis, the need for highly purified protein samples is paramount for such a quantitative approach. The traditional pH-based purification protocol has been shown to yield eluent samples of high ICER concentration, but fails to rid the solution of other proteins from cell extract, causing results that are somewhat accurate but suffer greatly from a lack of precision and

poor reproducibility. An imidazole-based, native purification provided the exact opposite scenario: eluent samples were extremely clean, but contained very little ICER as a result. Performing multiple titrations using natively purified ICER proved extremely difficult and time-consuming, and furthermore did not demonstrate any significant improvement on the issue of poor reproducibility.

Further experiments will necessitate examining the modified protocol using imidazole under denaturing conditions in greater detail, as the limited number of experiments performed using ICER samples prepared as such appeared to demonstrate binding comparable to what would be expected. However, the need to use heavily concentrated ICER to show binding in this scenario is extremely detrimental to performing any sort of useful binding studies using the binding models outlined earlier; thus, future work on this project will center around optimizing the purification of ICER using this method in order to allow for smaller concentrations to be used for binding studies. If successfully achieved, an extremely pure ICER sample that binds to the CARE sites at the expected concentration and does so reproducibly, should allow for large-scale analysis of binding studies, which could not only produce reasonable and reliable dissociation constants of single binding sites, but also open up the possibility of exploring the potential of cooperativity with the presence of multiple CARE sites and determine the mechanism of autoregulation by ICER.

Part Two: ELECTROCHEMICAL PROPERTIES OF TRYPTOPHAN

Introduction

Photolyase is a DNA repair enzyme whose structure and function are of burgeoning interest in the scientific community. Present in many organisms such as bacteria, goldfish, rattlesnakes, and marsupials, photolyase detects and repairs damage in DNA caused by exposure to UV radiation (22, 23). Given the continual chemical degradation and thinning of the ozone layer, this enzyme may have great importance in the future as a method by which humans and other organisms may protect themselves from harmful UV rays, and to a broader extent, a method of preventing skin cancer. Indeed there have been studies that demonstrate the effectiveness of algal lotions containing photolyase (humans and other placental mammals do not produce the enzyme) on protecting and repairing sunburnt human skin (24, 25). A related protein, cryptochrome, has been shown to transduce signals critical for growth, development, magnetosensitivity, and circadian rhythms (i.e., adaptive responses to UV and blue light exposure) in various organisms, although the mechanisms by which these phenomena occur are far less understood those of damaged DNA repair (26).

E. coli photolyase and other photoreceptors in the photolyase and cryptochrome family share a common structural motif. They are monomeric proteins typically around 500 amino acids in length, weighing ~55 kDa, and contain a flavin domain with two specific cofactors that can be photoactivated, shown in Figure 14: the flavin cofactor, FAD, the necessary cofactor for binding to and catalyzing the repair of damaged DNA; and the pterin cofactor, 5,10-

methyltetrahydrofolate polyglutamate (MTHF), which is not required for catalysis and has little effect on DNA binding specificity (22). Crystal structures of *E. coli* photolyase have been determined, as shown in Figure 15, and show two well-defined domains, one being an N-terminal α/β domain 130 residues in length, and the other a C-terminal α -helical domain of around 270 residues in length (22).

Photolyase requires the reduced FAD cofactor (FADH^-) for DNA repair. If the FADH^- cofactor is oxidized to its neutral radical form, FADH^\cdot , it can undergo subsequent photoreduction to give the active FADH^- . The mechanism of photoreduction of *E. coli* photolyase has been previously studied and continues to be examined due to its uniqueness for studies of protein electron transfer in enzymes. This portion of the master's thesis will focus on the study of this specific electron transfer mechanism that involves proton-coupled electron-transfer (PCET), and more specifically, the involvement of a particular solvent-accessible amino acid residue, ^{306}Trp , in the overall mechanism, also shown in Figure 15. Previous studies have determined that upon excitation, FADH^\cdot is reduced by oxidizing ^{306}Trp in the process shown in Figure 16, part A (27), and exogenous electron donors subsequently reduce the oxidized tryptophan, stabilizing the FADH^- and allowing for the enzyme to perform its DNA repair function (28, 29). Without exogenous electron donors, FADH^\cdot and Trp^\cdot undergo back-electron transfer through a PCET mechanism (30, 31).

Upon further investigation, evidence has emerged suggesting that as the pH of the surrounding environment increases, there may be a switch from a concerted electron proton transfer (CEPT) to an electron transfer followed by a proton

transfer (ETPT) between FADH⁻ and ³⁰⁶Trp; the basis for this switch in electron transfer mechanism is rooted in maintaining the most favorable balance between activation energy (ΔG^\ddagger) and driving force (ΔG) for the FADH⁻ cofactor and ³⁰⁶Trp upon completion of the transfer (31). In other words, at low pH values when the presence of free protons in solution is abundant, a CEPT mechanism is most energetically favorable, whereas an ET(PT) mechanism represents the lower-energy pathway at higher pH values in which there are significantly less protons in solution.

A mathematical context for this mechanistic switch, as a function of pH, has been provided by Hammarström and colleagues in a series of published articles examining a PCET mechanism in Ruthenium model compounds (32-35). Their particular model is used to investigate electron transfer of tyrosine using light-induced reactions, in which the ruthenium-tris-bipyridine part acts as a photosensitizer, the excited state is subsequently quenched by electron transfer to an external acceptor molecule, and an electron is then transferred to the oxidized ruthenium from the tyrosine that was originally deprotonated (34). In this sense, their electron transfer mechanism provided a viable paradigm, on which the studies in this thesis have been modeled both conceptually and mathematically. They used the Marcus theory of electron transfer with a correction for the change in entropy due to proton release. Marcus theory (35) describes the rate of electron transfer, k_{ET} , as shown in Equation 7, where: h is Planck's constant, k_B is Boltzmann's constant, H_{AB} is the electronic coupling matrix element, λ is the reorganization energy, and ΔG^0 is the change in standard free energy.

As mentioned previously, global analysis of the electrochemical and physical data from previous studies of the photoreduction of $\text{FADH}\cdot$ and charge recombination process by our research group substantiate the hypothesis that the electron transfer process follows a CEPT mechanism, with a switch to a sequential ET(PT) mechanism occurring around pH 6.5. Figure 16, part C provides a visual comparison of the two mechanisms as proposed by our group (31). In addition, part B of Figure 16 shows a proposed mechanism by Byrdin et al (30) that provided a foundation for our research and conclusions derived thereof. The mathematical analysis of voltammetric data and relevant kinetic parameters is shown in Table 2, below in which the proposed mechanism switch at pH 7.0 from a CEPT to the ET(II) mechanism is described by global fit parameters. It is most crucial to note that while the actual mechanism in play may still be debated, in all of these cases it is agreed upon that the rate of the charge recombination mechanism is largely reliant on the presence of protons in solution. In other words, the reaction rate is inversely pH-dependent—thus, the reaction is fastest at lower pH values and decreases as the pH of solution is increased (28, 30, 36).

In addition to studying the effects of pH changes on the electron transfer mechanism, all experiments of the entire range of pH were performed in two different solvents: distilled water, and deuterium oxide. Just as the change in proton availability with solution pH greatly affects the energy of reorganization following electron transfer, changing from distilled water to a heavier solvent such as D_2O will also create such a result. These different solvent effects (mass-related kinetic isotope effect, and solvent isotope effect) partially give rise to changes in charge

recombination energies when a proton transfer is involved, in which the specifics of the reaction in question will determine which specific solvent effect is most prevalent.

The particular isotope effects that will influence the rate of a reaction are largely dependent not just on the reaction in question, but also the level of participation of solvent molecules as reactants. The so-called "kinetic isotope effect", for example, occurs as a result of the isotopic exchange of solvents like replacing distilled water with deuterium oxide. When the isotopic replacement occurs in a chemical bond that is created or destroyed in the rate-limiting step of the reaction, this is known as a primary isotope effect, and a secondary isotope effect refers to such an isotopic substitution that is not directly involved in the rate-limiting step, which causes a smaller rate change than a primary effect (37). The primary isotope effect actually increases the activation energy of the reaction and only affects the rate-limiting step and no other steps. Additionally, reaction rates are always reduced when switching to a heavier solvent if there is only a primary kinetic isotope effect, whereas secondary kinetic isotope effects can result in either that traditional scenario or also the "inverse" effect in which heavier solvents raise the rate of reactions by lowering activation energy of parts of the reaction that are specifically not involved in the rate-limiting step of the mechanism (38). In the latter case, the solvent isotope effect would play an important role.

Both classical and quantum mechanical principles go into the principle of the phenomenon shown by the kinetic isotope effect. From a perspective of typical enzyme kinetics, there exist certain requirements in order for a kinetic isotope

effect to manifest itself in a particular mechanism: either the initial or final states (or both) must have a nonzero free energy of transfer, and those two values cannot be equal (39). Given that the kinetic isotope effect tends to display as a change in those two values, it actually results in a change in activation energy (somewhat indirectly) as well. A change in the free energy of transfer as the transition state is formed tends to carry over into the transition state itself, but not past this step, therefore the amount of change to the final state free energy of transfer caused by the kinetic isotope effect is, in effect, the change in activation energy as well (39).

Furthermore, the solvent isotope effect also influences several other thermodynamic parameters, such Gibbs free energy, enthalpy, entropy, and heat capacity change (40), as well as kinetic factors including pK_a of weak acids, reduction potential, and H-bonding (publications indicate it is stronger in D_2O) (31, 39, 40). More expressly, the presence of the different isotopes modify reaction rates based on their respective weights—thus, the effects are related to the change in vibrational frequencies of affected bonds, in which the general trend is heavier solvents will result in smaller vibrational frequency and zero-point bond energy, subsequently increasing the required activation energy to break bonds and lowering reaction rates (41). In this sense, a typical observed kinetic isotope effect when comparing distilled water and deuterium oxide is for a reaction to occur more slowly in the heavier solvent, i.e. D_2O . In observed primary kinetic isotope effects, the reaction rate can decrease by up to a factor of seven when replacing hydrogen with deuterium, whereas secondary effects, both traditional and “inverse” (see below), typically only manifest themselves in factors of two or less (42, 43).

However, while this is the most common effect, there are many mechanisms that actually follow the opposite scenario; that is, these reactions show an increased rate in heavier solvents. This particular effect is known as an “inverse” isotope effect, and has been observed in the previously published study of charge recombination following photoreduction of FADH \cdot that this portion of the thesis is largely based on. Indeed the voltammetry experiments from this work are measuring and explaining this specific phenomenon in greater detail. This may seem counterintuitive, in that the CEPT mechanism occurring at the lower pH values should be governed, in theory, by a mass-related kinetic isotope effect in switching from distiller water to deuterium as a solvent. In fact there appears to be a combination of two effects that manifests itself in the shift of voltammetric results, both the above-mentioned mass-related isotope effect and the “inverse” effect, described below, which accounts for the experimental results that show how the charge recombination mechanism actually takes place more quickly and easily in the heavier deuterium-based solvent than distilled water itself (30, 31).

This so-called “inverse” kinetic isotope effect, i.e. the increase in reaction rate when replacing distilled water with deuterium oxide, is observed in the photoreduction of FADH specifically at and below pH/D 8 as shown in Figure 17, and has been proposed to be due to the Trp redox potential as well as specifics of this particular reaction mechanism, such as the pK $_a$ of the Trp residue of interest (31). Analysis of enzyme-catalyzed reactions such as the photoreduction of FADH \cdot is still possible in spite of the existence of both effects, as secondary isotope effects due to the presence of hydrogen (or lack thereof), and the resultant reaction rate

changes, will certainly result in changes in measured redox potential: as proposed in the previous study of this reaction mechanism (31), the observed "inverse" deuterium effect appears to be due to a solvent isotope effect that affects the Gibbs free energy change (ΔG) and, to a lesser extent, the reorganization energy (λ) of the reaction at pH values at and below 7.0.

In this work, we will test the hypothesis that the redox potential of tryptophan increases in D_2O as compared to H_2O by using cyclic voltammetry and differential pulse voltammetry.

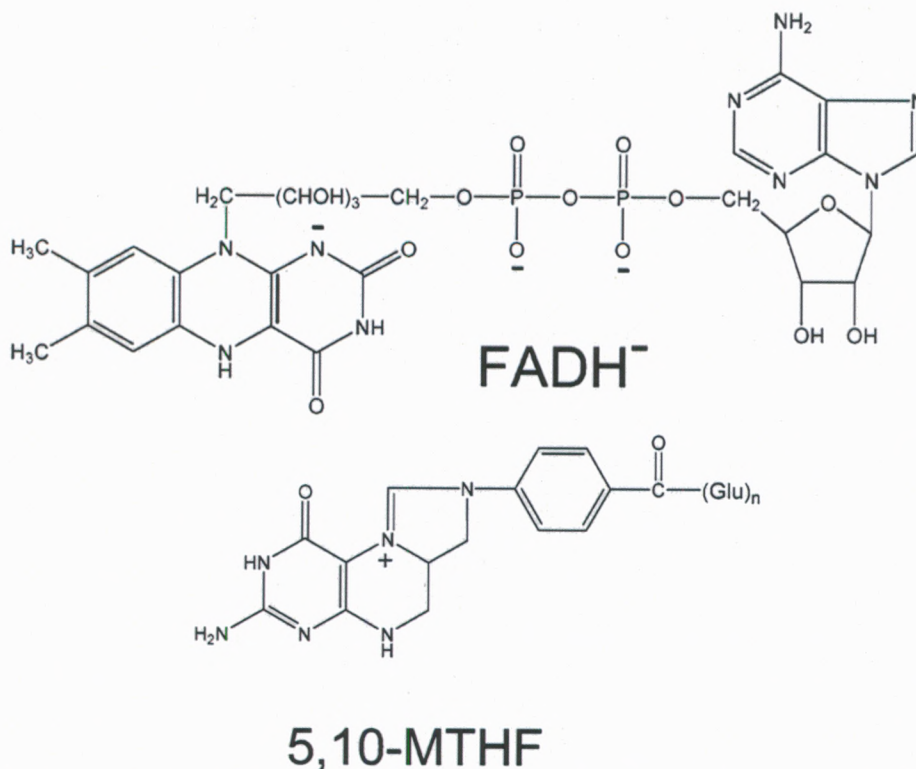


Figure 14. Structures of the FAD and MTHF cofactors in photolyase. The reduced form, FADH⁻, is shown, as is the positively charged MTHF. The 'n' in the MTHF structure represents an indiscriminate number of glutamine residues attached to the carbon, which can range from 1-5, or more in some cases (22).

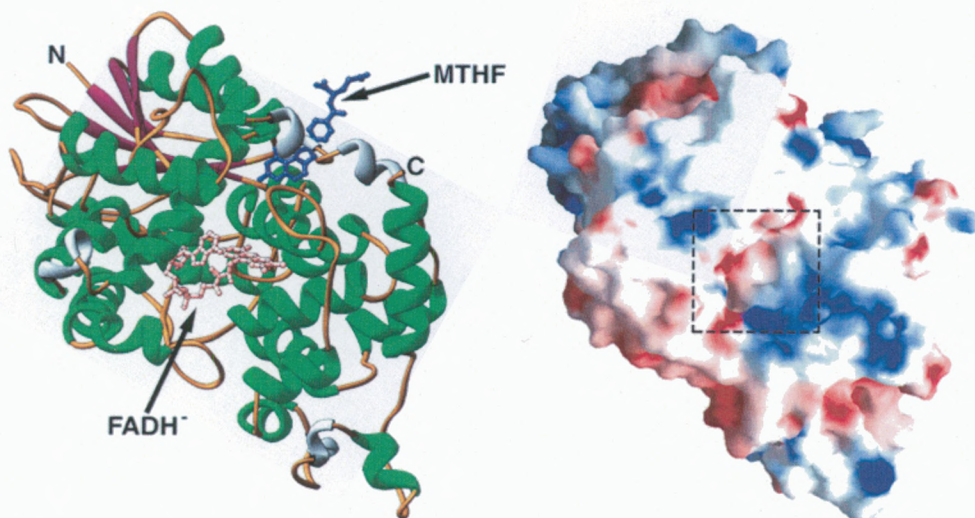


Figure 15. Crystal structure of *E. coli* photolyase. Ribbon diagram on the left shows the position of each cofactor, and the domains at each terminus. Surface potential representation shows solvent-exposed residues (blue: basic groups, red: acidic groups, white: hydrophobic groups). ³⁰⁶Trp is one of the solvent-exposed residues (22).

$$k_{ET} = \frac{2\pi}{\hbar} \frac{H_{AB}^2}{\sqrt{4\pi\lambda k_B T}} \cdot \exp\left(-\frac{(\Delta G^0 + \lambda)^2}{4\lambda k_B T}\right)$$

Equation 7. Marcus theory of electron transfer. Parameters of interest are in exponential portion.

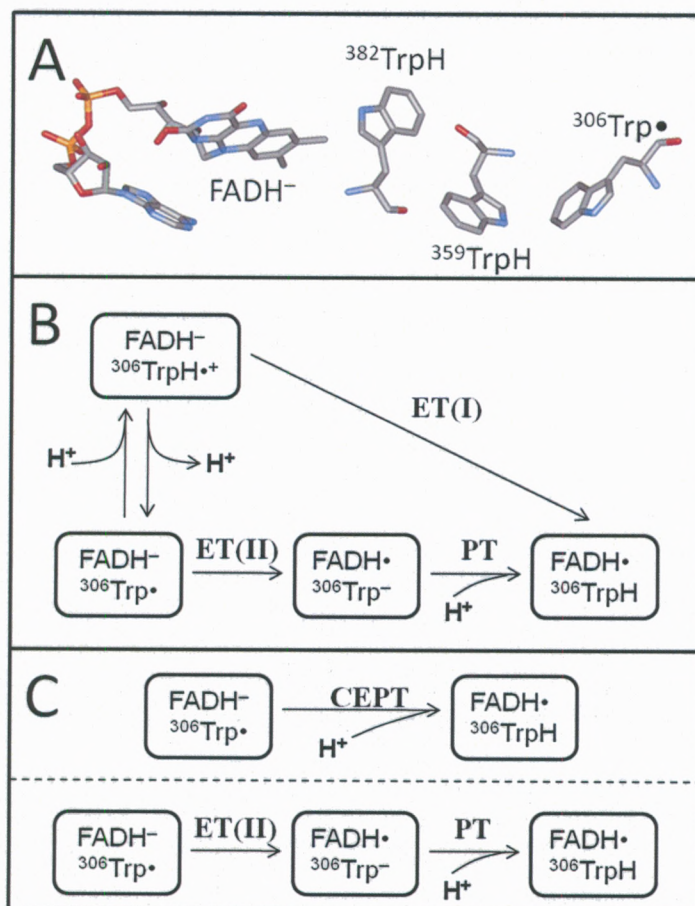


Figure 16. Proposed mechanisms of photoreduction of FADH and charge recombination in *E. coli* photolyase. Part A shows the flavin cofactor in its reduced form, and sequence of tryptophan residues involved in the electron transfer including the radical form of ^{306}Trp ; Part B is the mechanism proposed by Byrdin et al (30); Part C shows the two mechanisms as proposed by our research group (31). The CEPT mechanism is proposed to occur at lower pH values, with the sequential ET(PT) mechanism taking over at pH 6.5 and higher.

	$E_m^0(\text{FADH}^-/\text{FADH}\cdot)$ (mV)	$E_m^0(\text{Trp}\cdot/\text{TrpH})$ (mV)	ΔS_{uptake} (eV/K)
CEPT	12.25 (45) ^a	$1070 - [\text{pH}(D) - \text{pK}_a] \cdot 53^b$	$-\text{Rln}(10)\text{pH}(D)$
ET(I)	12.25 (45) ^a	1070 (1070) ^a	0
ET(II)	12.25 (45) ^a	365 (395) ^a	0

Table 2. Thermodynamic parameters used for the Global Analysis Fit to the Two Electron Transfer Models in H_2O and D_2O solutions (30). ^aValues for D_2O are given between parentheses; ^b $\text{pK}_a = 3.7$ and 4.26 in H_2O and D_2O , respectively.

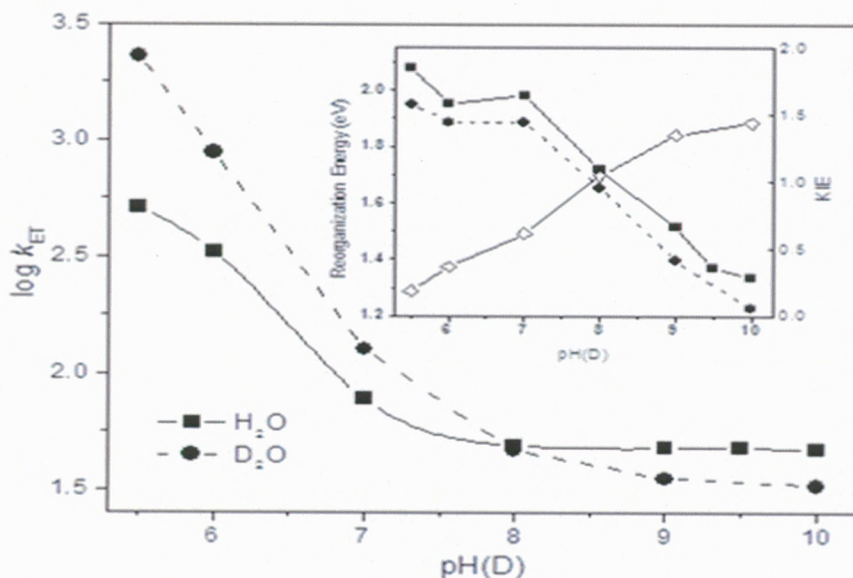


Figure 17. Rate of charge recombination in photolyase as function of pH(D) in H_2O and D_2O solutions (10). Inset: kinetic isotope effect as function of pH(D) .

Materials & Methods

Study of Isotope Effects. It would be unrealistic to break down and specifically examine all of the abovementioned kinetic and thermodynamic parameters that arise as consequences of the kinetic isotope effect, so these experiments primarily focus on the comparison of the reduction potential of tryptophan in the two solvents, which is a term that allows for broad analysis of several other parameters of the mechanism as a result. The key parameter that affects the electron transfer rate is the activation energy, which is given by Equation 8. As indicated in Equation 9, the Gibbs free energy of reaction (ΔG) is mathematically defined as the difference between the reduction potential of the FADH cofactor, and that of ^{306}Trp . Furthermore, Equations 10 and 11 demonstrate

the relationship between ΔG of reaction and several other relevant experimental parameters: reorganization energy, λ , activation energy, ΔG^\ddagger , pH/pD of solution, pK_a of Trp, all of which play critical roles in the determination of the rate (k_{CEPT}) of the electron transfer process, where pK_a and pK_a^D are the pK_a of the tryptophan radical in H_2O and D_2O , respectively.

Since our research group's previous study concluded that the kinetic isotope effect is negligible to the reorganization energy parameter of the reaction (27), it follows that any changes in reaction rate due to using D_2O (both "expected" and "inverse") is most expressly due to the resultant change in the Gibbs free energy change. An anticipated consequence of replacing distilled water with the heavier solvent D_2O is an increase in the reduction potential of the $FADH\cdot$ cofactor, which was also observed in our group's previous study. Indeed this kinetic isotope effect, while small, still appeared, causing a slight increase in ΔG of the reaction, raising the energy of activation, and decreasing the rate accordingly. Nonetheless, as the data in this thesis establishes, this small kinetic isotope effect is not only negated, but also overridden by the apparent "inverse" solvent isotope effect.

Again, as shown in Equations 7 - 11, this "inverse" effect is postulated to be due to a significant increase in the reduction potential of tryptophan (as a model for ^{306}Trp) (31), which itself is affected by solution pH. Therefore, a series of experiments were performed at specifically predetermined intervals over a wide pH range to explicitly determine the quantitative relationship between solution pH and ^{306}Trp reduction potential in distilled water, then repeated in D_2O , to assess our research group's hypothesis and possibly give credence to our proposed

explanation for the observed "inverse" solvent isotope effects. Additionally, the experiments were repeated using two molecules shown in Figure 18: L-Tryptophan as a free amino acid, and a tryptophan analog, N-acetyl-L-tryptophanamide which artificially includes an amine group that replaces the hydroxyl group on the C-terminus, and an added acetyl group to the N-terminus. Both chemicals were purchased from Sigma-Aldrich and used without further purification. D₂O was purchased from Cambridge Isotope Laboratories, Inc.

Part of the theoretical basis behind using the tryptophan analog is to prevent both traditional amino acid ionization steps from occurring, which would theoretically eliminate the possibility of changing electrostatics of the molecule causing experimental error. In theory, the tryptophan analog also would allow for measurements to occur over a wider pH range than the free amino acid itself, again due to the elimination of the two pK_a's at 2.46 and 9.41. In addition, replicating the conditions of a previous study of the electrochemistry of N-acetyl-L-tryptophanamide as a radical-forming electron-transfer cofactor would allow for further analysis and comparison of the experimental results (44). Lastly, due to the extremely small numerical scale involved in this analysis, and the sensitivity of the electrochemical measurements, all experiments (described in greater detail below) were each performed multiple times in order to minimize any possibility of experimental error and determine the statistical significance of the results.

Electrochemistry. Given that the mechanism of interest involves electron transfer and redox potential, and the effect being studied is pH dependent, it follows that voltammetry is a practical analytical method for examining the redox potential

of such a reaction. Voltammetry broadly refers to a category of electrochemical methods that explore the half-cell reactivity of a particular analyte, specifically by measuring the current of a solution while varying an applied potential (45). The resultant graphs, known as voltammograms, depict current as a function of potential over a predetermined time span, and differ in appearance based on the specific technique being used. One such technique particularly useful for gathering redox information of an electron transfer mechanism, such as rate constants, is cyclic voltammetry.

Cyclic Voltammetry. In this method, experimental conditions are manipulated in such a way that the kinetics of electron transfer become competitive with the rate of potential change; under such conditions, sample reduction and oxidation peaks are elucidated, and the separation of peak potentials is a reasonable measure of the standard rate constant of electron transfer as it is a calculable function of frequency at this peak potential separation (46). In other words, electrode potential ramps, or “sweeps”, linearly as follows: first, applied potential is initially ramped up (i.e., anodic current) to show a sample reduction peak, then subsequently inverted and scaled back down to its initial level (i.e., cathodic current) to elucidate a sample oxidation peak (47), and the resultant voltammogram depicted in Figure 19 contains information about the redox potential and electrochemical kinetics of the analyte. All L-Tryptophan experiments were performed using cyclic voltammetry and followed experimental parameters as detailed in a previous study by this research group (31), again to allow for more detailed analysis and comparison of these results. Although the reaction is a full

oxidative-reductive process, due to the extremely limited time scale of the reaction, cyclic voltammetric experiments only yielded an oxidation peak in the forward sweep direction and completed before the backwards voltage sweep occurred. This required the application of a mathematical correction factor prior to data analysis, as described later.

Differential Pulse Voltammetry. Similar to cyclic voltammetry is another electrochemical method known as differential pulse voltammetry. While both techniques will ostensibly provide the necessary information required for quantitative analysis, differential pulse is slightly different in terms of how the current/voltage relationship is applied over the course of the experiment. While cyclic voltammetry sweeps the desired voltage range linearly in both forward and reverse fashion, the differential pulse technique goes through the voltage range by intermittently "pulsing" at predetermined voltage intervals, and this series of voltage pulses replaces the linear sweep shown in cyclic voltammetry (48). Furthermore, as Figure 20 shows, differential pulse will only scan in the forward direction of the voltage range, as opposed to both forward and backwards. In theory, this technique should be more sensitive and precise because the entire process takes place over a smaller time scale, and minimizes the effect of the charging current by sampling the total current as late as possible after the application of each potential pulse (49). All N-acetyl-L-tryptophanamide experiments were performed using differential pulse voltammetry.

Redox Standard Couple. In order to provide numerical context to the peak potential values of L-tryptophan and N-acetyl-L-tryptophanamide in solution, it is

imperative to use an external standard of 10.0 mM potassium ferricyanide ($\text{K}_3\text{Fe}(\text{CN})_6$) in 0.2 M KCl. This standard couple, shown in Figure 21, is particularly effective for electrochemical measurements largely due to its molecular properties: the ferricyanide ion has octahedral symmetry, and is a low spin complex—therefore it is easily and reversibly reduced to ferrocyanide by single electron transfer making for an efficient redox couple that is widely used as a standard for voltammetric analysis (50).

pH-dependent Study. While this charge recombination process for photolyase has documented small temperature dependence as well (27), this thesis only focuses on the effect of pH changes on the rate constant of the process, instead of the contribution from both parameters. Thus, each and all voltammetric measurements were taken at the same temperature (i.e., a temperature-controlled laboratory) and compared against the same standard solution, in order to ensure that, within reasonable experimental error, the only parameter that was changed was the pH/D of the solutions. For the set of experiments in L-Tryptophan, a pH/D range of 3.0-8.0 was used, with measurements taken at every increment of 0.5 pH/D units. For N-acetyl-L-tryptaphinamide, measurements were again taken at 0.5 pH/D unit increments, but the range of pH/D was extended from 2.0 to 10.0.

Buffer Solutions. Electrochemical experiments were performed in a buffer solutions prepared containing each of the following compounds, in which only the solvent itself was changed for each set: 10.0 mM citric acid; 10.0 mM potassium phosphate dibasic trihydrate; 10.0 mM sodium pyrophosphate; 10.0 mM succinic acid; 10.0 mM Tris buffer; 0.2 M KCl. The presence of KCl is to act as a relatively non-

reactive background electrolyte that allows for current flow but does not exhibit absorption at the electrode surface or otherwise interfere with measurements. From a total prepared stock buffer of 500 mL, an aliquot of 25 mL was extracted and 10.0 mM of either L-Tryptophan or N-acetyl-L-tryptophanamide was added. Each aliquot pH was set accordingly using a 1.0 M HCl solution diluted from a concentrated stock or a 1.0 M NaOH solution prepared from solid NaOH pellets. For the D₂O experiments, the NaOH solution was prepared in D₂O, and the 1.0 M HCl was prepared from the same concentrated stock and diluted using D₂O. In accordance with previous publications, it has been shown that the pH meter reading in D₂O solution is 0.40 pH units lower than in H₂O (51); therefore, this shift was taken into when setting the pD of those solutions. For example, to set a solution to pD 4.0, the solution would be set to show a pH reading of 3.6 on the meter.

Instrumentation. Once the aliquot of requisite pH/D and protein concentration was prepared, it was taken to the temperature-controlled electrochemistry lab for voltammetric analysis. All electrochemical data was taken using the CH Instruments 660C Electrochemical Workstation and Picoamp Booster & Faraday Cage, using the accompanying software to set parameters and produce voltammograms. In accordance with the commonly used three-electrode system detailed in Figure 22, the reference electrode was glassy carbon electrode containing KC; the counter electrode was gold; and the working electrode was palladium. For the L-Tryptophan experiments run using cyclic voltammetry, the experimental parameters were as follows: initial voltage: -0.4 V; low voltage: -0.4 V; high voltage: 0.8 V; Positive Initial Scan Polarity; Scan Rate: 0.06 V/s; Sweep

Segments: 2; Sample Interval: 0.001 V; Quiet Time: 2.0 s; Sensitivity: 10^{-5} A/V. Differential pulse voltammetry experiments for N-acetyl-L-tryptophanamide were performed under the following conditions: initial voltage: -0.4 V; high voltage: 0.8 V; voltage increment: 0.004 V; amplitude: 0.05 V; pulse width: 0.05 s; sampling width: 0.0167 s; pulse period: 0.2 s; Quiet Time: 4.0 s.

It was necessary to purge each aliquot with nitrogen gas for a minimum of 3-5 minutes prior to each trial in order to eliminate the presence of oxygen in solution, which would otherwise be oxidized and appear as a very large peak on each voltammogram. Likewise, prior to each trial, both the counter and reference electrodes had to be cleaned thoroughly (typically while the aliquot was purged with nitrogen) to rid them of any crystallized materials from previous experiments. The electrodes were rubbed vigorously in a circular motion on a 9.0 cm Whatman silicon-treated phase separator circle that had been treated with 0.05 micron Gamma Alumina Powder from CH Instruments, and then rinsed several times in distilled water. After the cleaning process, all three electrodes were stored in distilled water for at least 3 minutes; at which point the standard redox couple measurements were taken.

Consistency in the appearance of the standard reduction peak was used as an indicator for successful cleaning of the reference and working electrodes for differential pulse experiments. For the cyclic voltammetry data, a difference of 0.080 V or less between the standard redox couple oxidation and reduction peaks served as such a gauge. Again, standard measurements were also taken before each individual trial, as quantitative analysis of all subsequent electrochemical data

warranted the gathering and recording of such information. Lastly, a control experiment was performed in duplicate in which the standard solution was prepared in both solvents and subjected to the same electrochemical analysis. This was to ensure that the electrochemical properties of the standard redox couple were not affected by a change in solvents and that any observed changes of the reduction potential of the two molecules of interest were consequential to solvent effects alone. In other words the control experiment was chiefly performed to ensure that the sole parameter that would change from one trial to another was the pH/D of solution.

$$\Delta G^\ddagger = (\Delta G^{0t} + \lambda)^2 / 4\lambda.$$

Equation 8. Activation energy of electron transfer mechanism, combining Gibbs free energy (ΔG^{0t}) and reorganizaion energy (λ) parameters.

$$\Delta G^0 = e[E_m^0(FADH^- / FADH^\bullet) - E_m^0(Trp^\bullet / TrpH)]$$

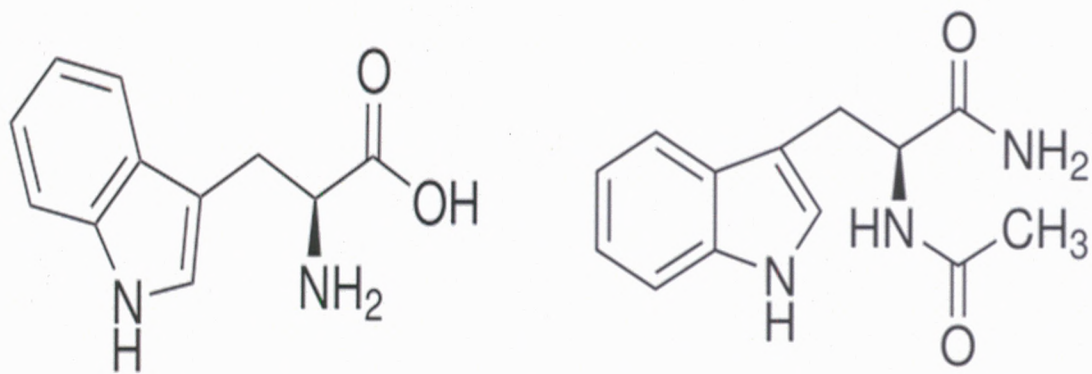
Equation 9. Relationship between Gibbs free energy term and reduction potentials of FADH cofactor and ^{306}Trp residues. Difference between FADH cofactor reduction potential and that of ^{306}Trp mathematically determines Gibbs free energy.

$$E_m^0(Trp^\bullet / TrpH) = 1070 - (pH - pK_a) \cdot 53 \text{ mV}$$

Equation 10. Reduction potential of Trp in H_2O .

$$E_m^0(Trp^\bullet / TrpD) = 1070 - (pD - pK_a^D) \cdot 53 \text{ mV}$$

Equation 11. Reduction potential of Trp in D_2O .



L-TRYPTOPHAN

N-ACETYL-L-TRYPTOPHANAMIDE

Figure 18. Structures of the two molecules used in electrochemical experiments. Note addition of the amine group on the C-terminus and addition of acetyl group on N-terminus to the tryptophan analog on right. Artificial inclusion of these functional groups prevents the protonation or ionization of both termini, thereby eliminating the possible effects on experimental results that the changing electrostatics of the molecule could potentially cause as the pH is changed.

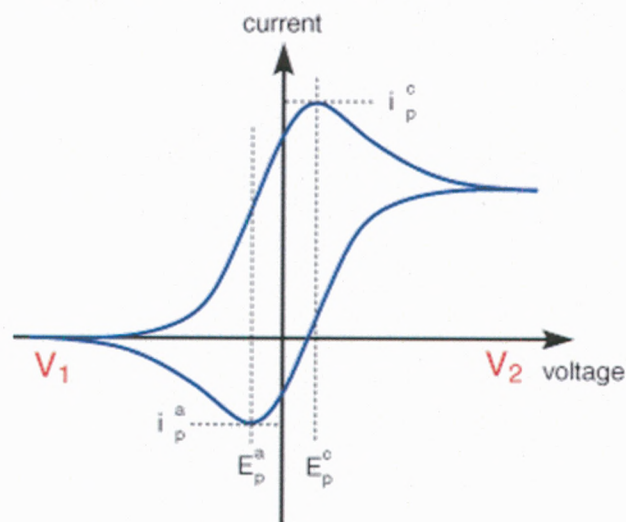


Figure 19. Generic cyclic voltammogram. i_{ap} and i_{cp} show, respectively, peak cathodic current (reduction peak) and anodic current (oxidation peak), whereas E_{ap} and E_{cp} denote the voltages at which the two peaks occur along the linear sweep. V_2 is the starting (and ending) voltage, and V_1 is the voltage at which the sweep is inverted. (Department of Chemical Engineering & Biotechnology, University of Cambridge. Linear Sweep and Cyclic Voltammetry: The Principles. <http://www.ceb.cam.ac.uk/pages/linear-sweep-and-cyclic-voltammetry-the-principles.html> (accessed 3/20/2012).)

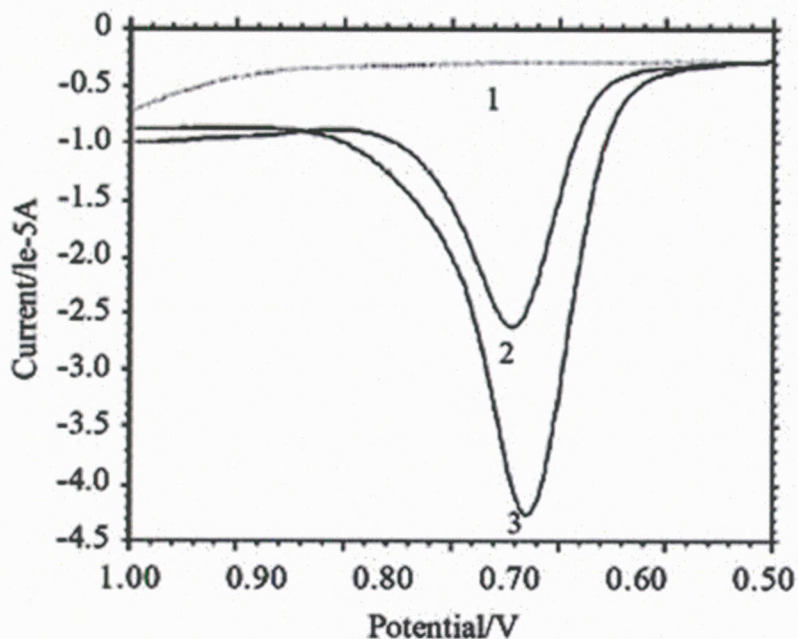


Figure 20. Generic differential pulse voltammogram. Contains three experiments of varying concentrations of the same analyte. The peak amplitude is proportional to concentration. (Jin-Long, Y.; Xiu-Ping, Lu. *J. Chin. Clin. Med.* **2006**, 6 (1))

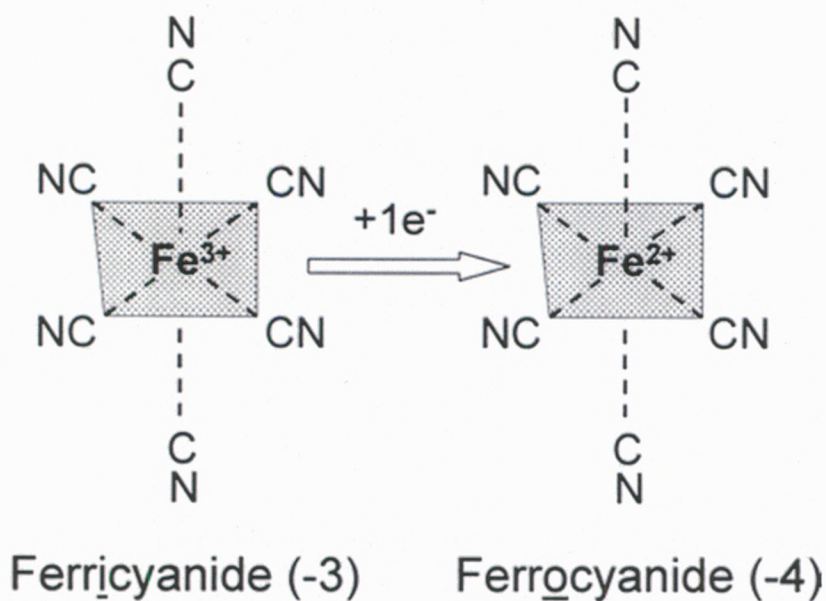


Figure 21. Reversible reduction of ferricyanide ion to ferrocyanide, i.e. the standard redox couple for all voltammetry measurements presented in this thesis. Octahedral symmetry is maintained for both ions, with electron transfer occurring to the low-spin iron. (May, James M. *FASEB Journal*, **1999**, 13 (9), 996)

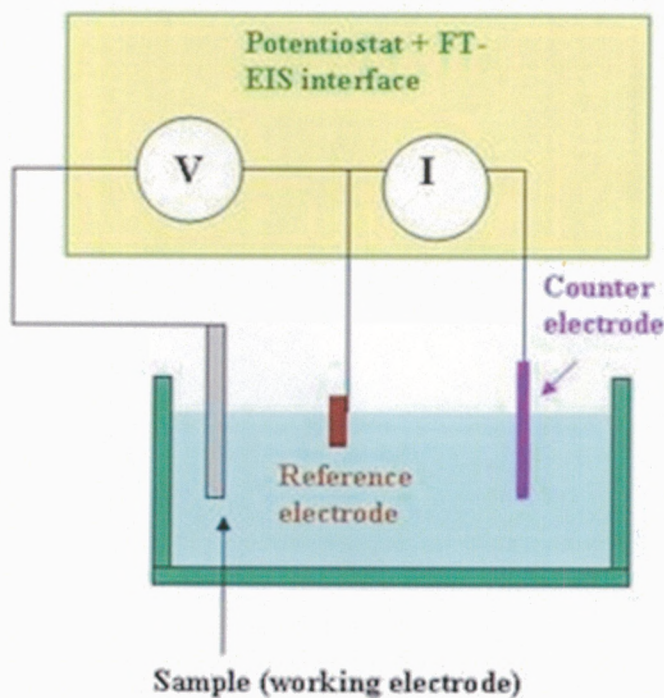


Figure 22. Three-electrode system. In the experimental system used for this thesis, glassy carbon electrode is the reference electrode, the counter electrode is gold (an electrically inert molecule), and the working electrode was palladium. (Roy Research Group. Corrosion monitoring using FT-EIS. <http://people.clarkson.edu/~droy/Corrosion EIS files/image004.jpg>. (accessed 4/24/12))

Results & Discussion

As previously described, the parameter of interest was the reduction potential of tryptophan in distilled water and deuterium oxide. An observed increase in this value for experiments in D_2O would support the postulate that the reason for a quicker reaction rate in the heavier solvent, i.e. the “inverse” solvent isotope effect, is in large part due to the increased tryptophan reduction potential, whose contributions to the Gibbs free energy of the reaction results in a larger electron transfer mechanism rate in D_2O , contrary to the expected consequences of

the kinetic isotope effect. Hence, experimental data that consistently displayed this phenomenon to a statistically significant level would be considered a successful endeavor in defending the original hypothesis. The most straightforward and easily visualized evaluation of all experimental data is to depict it in graphical form. Accordingly, x-y scatter plots were created for the set of experiments using L-Tryptophan and N-acetyl-L-tryptophanamide in which the observed reduction potential of the molecule in both H₂O and D₂O at each pH increment were plotted in the same graph. Four trials were run at each of these increments, and the average value is plotted for each increment. Error bars are shown at each data point representing the value of the standard error in the positive and negative directions and demonstrate the statistical significance of any observed "inverse" isotope effect, or lack thereof.

However, prior to making these graphs, it was necessary to apply some correction factors to the observed reduction potential values, which were applied individually to each data point. For the L-Tryptophan data taken using cyclic voltammetry, there were two such corrections. The first, correction 1, was used to account for the observed shift in the standard redox couple reduction peak relative to literature value of +360 mV (52), the value for which varies from one experimental setup and instrument to another. Standard reduction and oxidation peaks generally appeared around 0.220 V and 0.140 V, respectively, and the average redox potential of ferricyanide was about $(0.220 \text{ V} + 0.140 \text{ V}) / 2 = 0.180 \text{ V}$. The literature value of ferricyanide is 0.360 V, and a correction of +0.180 V is required to obtain the proper redox potentials. The correction was determined by measuring

ferricyanide before each tryptophan measurement and corrected appropriately by adding the correction of the specific standard measurement to the L-tryptophan reduction potential. The purpose of the second correction, correction 2, is to simulate the appearance of a peak from L-tryptophan in the backward sweep direction of each cyclic voltammogram, since the entire oxidative-reductive process happens too quickly to appear in the time it takes to run each voltage cycle. Acceptable standard oxidation peaks showed around 0.140 V, in accordance with the necessary <80 mV space; this space between standard peaks was halved (~40 mV), and then subtracted from each L-tryptophan reduction potential observed after that particular standard measurement, just as with the first correction. The resultant data point including both correction factors is referred to in the plot, Figure 23, as the standard midpoint potential. The total correction was shown in Equation 12, with typical values of correction 1 and correction 2 of 180 mV and 40 mV, respectively.

Analysis of the observed reduction potentials of L-Tryptophan in H₂O and D₂O as shown in Figure 23 reveals that the reduction potential in D₂O is considerably larger than in H₂O at every increment in the pH range. As the relationship between ³⁰⁶Trp reduction potential and reaction rate is described earlier, it is reasonable to state that these data provide strong evidence of a significant "inverse" solvent isotope effect present from pH 2.0-8.0, which not only cancels out, but also completely masks the expected mass-related kinetic isotope effect. This "inverse" solvent isotope effect has clearly manifested itself in the form

of a consistently observed increase in reduction potential in D₂O and, hence, a corresponding increase in reaction rate, k_{CEPT} , in the heavier solvent.

The pH-independent redox potential of 1.066 V in H₂O compares well to the value of 1.07 V determined by Tommos et al but not so well to the value of 1.015 V reported by Harriman (44, 53). Although the slope over the entire pH range is too small, it is -59 mV/pH between pH 4.5 and 6.5, and the pK_a is predicted to be 4.23. In D₂O, the pH-independent redox potential is 1.079 V, and the slope is -61 mV/pH and -62 mV/pH for the pH ranges of 4.5 to 6.5 and 5.0 to 6.5, respectively. The pK_a in D₂O ranges from 4.52 to 4.55. Therefore, D₂O causes an increase in the pH-independent Trp redox potential of +13 mV and an increase in the pK_a of 0.29 to 0.32. This is within the range of pK_a shifts in D₂O for weak acids (54-56). These values support the hypothesis that both the redox potential and the pK_a of tryptophan increase in D₂O and are responsible for lowering the activation energy and increasing the rate of charge recombination in photolyase at lower pH values (31).

However, the L-Tryptophan data was not all that perfect. Most incommodiously, the reduction potential of L-Tryptophan essentially "flattened out" in both solvents at the higher pH/D values, counter to what is theoretically and experimentally expected (31, 44, 53). This flattening out may be related to the ionization of the -NH₃⁺ group of tryptophan at higher pH values. Also, the "slope" of the pH vs. potential peak plot that arises from that same relationship is theoretically predicted to be -59 mV/pH and was determined to be -53 mV/pH in experiments (44). In our experiments, a slope of approximately -0.40 mV/pH unit was found in

the pH range (4.0-7.0) that displayed such a relationship. Indeed the results of the L-Tryptophan experiments can at least be considered in keeping with the postulated appearance of the "inverse" solvent isotope effect.

Differential pulse voltammetry only sweeps in one direction, and standard measurements only yield one reduction peak (similar in value to the other experiments) and, under ideal conditions, this peak is equivalent to the reduction potential. Therefore, it was only necessary to apply one correction to account for the observed shift in the standard peak relative to the literature value for the N-acetyl-L-tryptophanamide experiments. The difference between the observed standard peak for each individual measurement of ferricyanide and its literature value of +360 mV as a whole was added to correct the observed N-acetyl-L-tryptophanamide reduction potential, and the resultant data point including the correction is referred to in the plot, Figure 24, as the standard midpoint potential.

The data from the N-acetyl-L-tryptophanamide experiments are unfortunately not as successful or conclusive in that respect. Though the minuscule error bars in Figure 24 indicate the data is certainly precise, there is no apparent or statistically significant difference in the observed reduction potentials in the two solvents that trends throughout the entire pH range. The pH-independent redox potential (pH 2.0 - 4.0) is 1.013 V and 1.011 V in H₂O and D₂O, respectively. Although the values from pH 7.0 and upwards, especially starting at pH 8.0, show an increased reduction potential in D₂O, the effect is minimal or nonexistent over the rest of the pH range; in fact, results from the lower pH values would seem to suggest the presence of the mass-related kinetic isotope effect alone, however small, directly

contradicting both the proposition of the unique solvent effects this mechanism is subject to, and more importantly, the previously published data of the works that served as the foundation for this portion of the thesis.

The study by Tommos et al (44) supplied the framework to which the study of N-acetyl-L-tryptophanamide reduction potential could be compared, as their technique and experimental parameters were explicitly replicated for this express purpose. Unfortunately, there were also disparities between their and our results, as detailed in Figure 25. First, they measure a pH-independent redox potential of 1.07 V compared to ours of 1.013 V, which may hint at an error in our correction procedure due to the assumption that the molecule behaves ideally. Second, the reduction potentials “flattened out” from pH 8.0 and up, counter to the data taken by Tommos et al (44). Third, the shape of the graph in Figure 25, and the rate decrease or “slope” due to increasing pH was on the order of -53 mV/pH, whereas our experiments yielded a slope of approximately -40 mV/pH in that pH range (4.0-8.0). In the case of N-acetyl-L-tryptophanamide, the flattening of the reduction potential at higher pH values is unexpected because the absence of the -NH_3^+ should have prevented this from occurring. It may be that the purity of the material was not sufficiently high and that the presence of some impurities caused the unexpected pH dependence of the reduction potential.

$$E_m(\text{Trp}\cdot/\text{TrpH}) = E_m(\text{Trp}\cdot/\text{TrpH}) + \text{correction 1} - \text{correction 2},$$

Equation 7. Application of two correction factors to observed Trp reduction potentials. Resultant data referred to as standard midpoint potential.

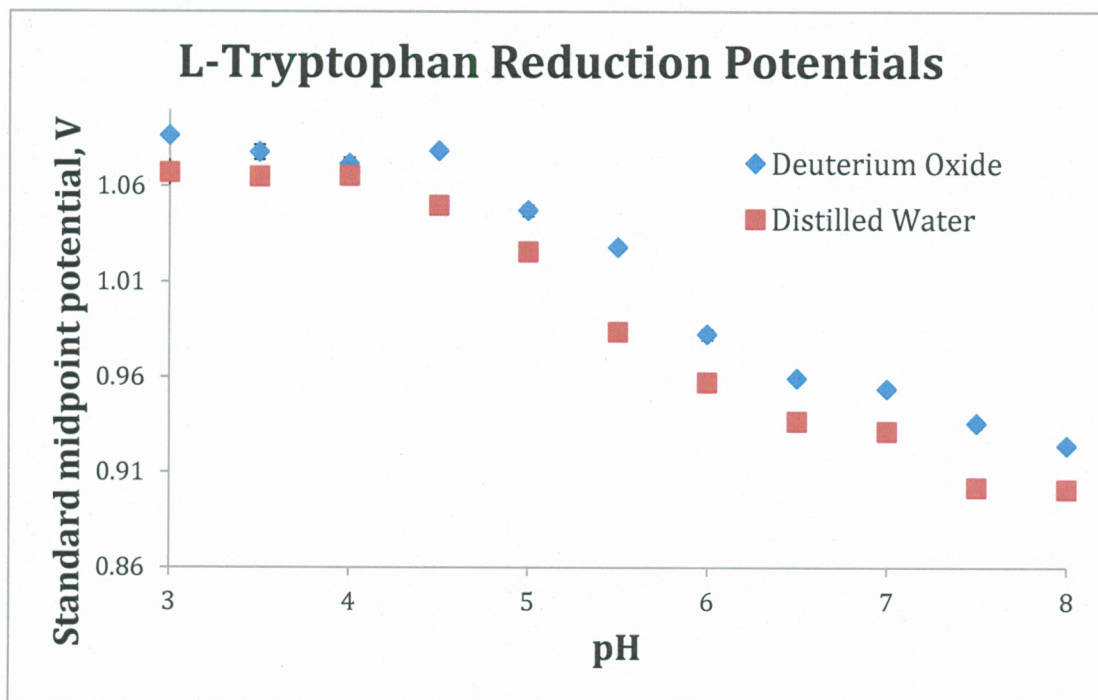


Figure 23. Standard midpoint potential of L-Tryptophan in H₂O and D₂O as a function of pH.

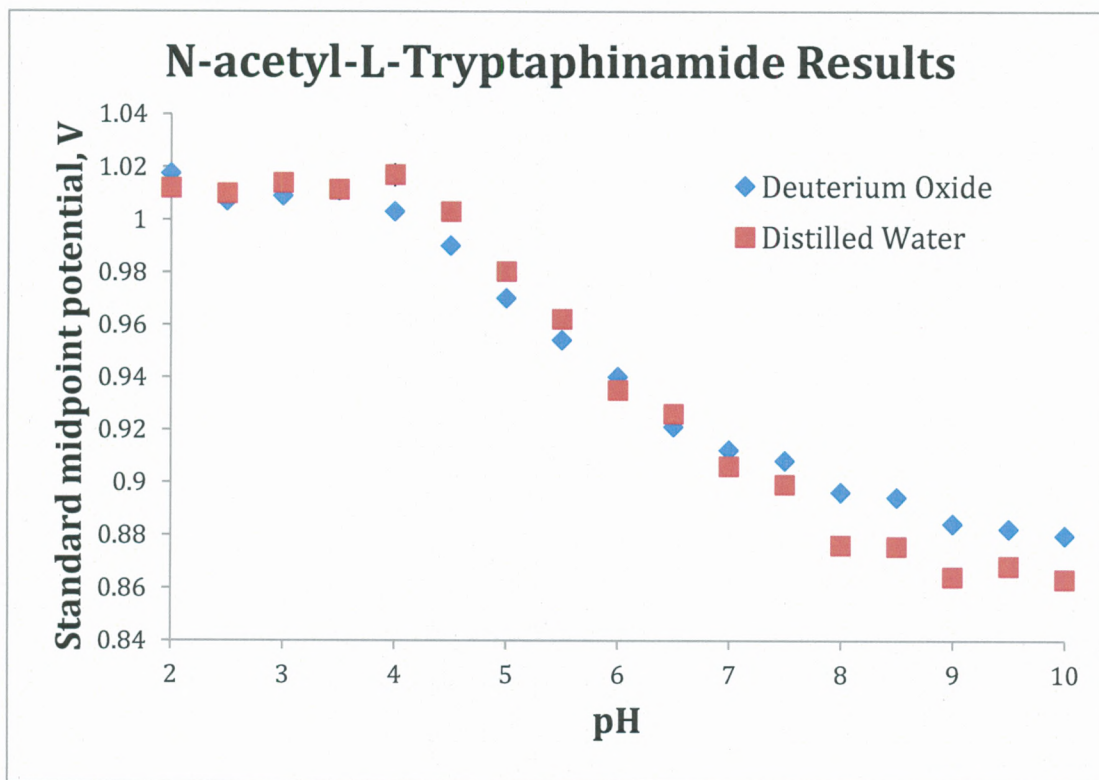


Figure 24. Standard midpoint potential of L-Tryptophan in H₂O and D₂O as a function of pH.

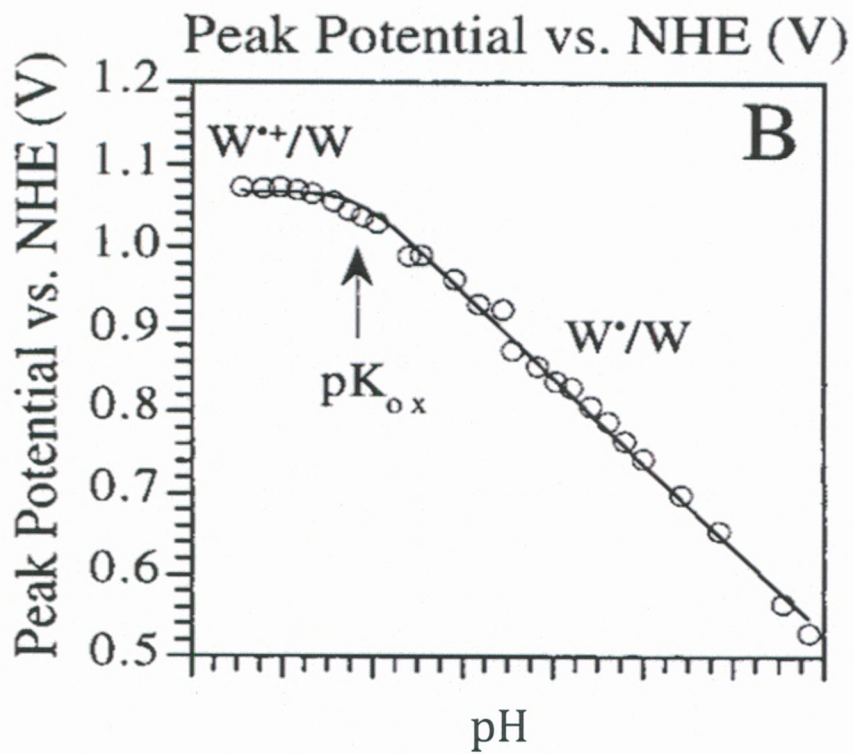


Figure 25. Graph of N-acetyl-L-tryptophanamide peak potential in H₂O as a function of pH from differential pulse voltammetry experiments (43). Scale of x-axis is pH 0.0-10.0.

Conclusion

This portion of the thesis focused on electrochemical analysis of the specific electron transfer mechanism governing FADH \cdot photoreduction in *E. coli* photolyase, the involvement of amino acid ^{306}Trp in the mechanism, the effects of solution pH and, most specifically, determining the effects of using a heavier solvent, D $_2$ O, on the rate of electron transfer. The experiments detailed herein most specifically sought to explain the observation of an increased reaction rate in D $_2$ O, which our research group postulated is the result of an “inverse” kinetic isotope effect. This directly contradicts the expected impact of using a heavier solvent, known as the mass-related kinetic isotope effect, which causes the reaction to slow down.

In building upon and utilizing previously published work by this research group and that of fellow scientists for experimental setup and data comparison (30, 31, 44, 53), the data compiled from these experiments were expected to demonstrate a consistently higher reduction potential of L-Tryptophan and N-acetyl-L-tryptophanamide in deuterium oxide, which as previously described, is directly related to the observed “inverse” kinetic isotope effect. By conducting these experiments over a wide range of pH/D, it was possible to also observe the effect of pH/D on the redox potentials and compare the data to previous studies.

Whereas the experiments using L-Tryptophan in D $_2$ O showed an increased reduction potential over the entire pH range, giving credence to our research group’s proposed explanation of the “inverse” kinetic isotope effect (31), the data from N-acetyl-L-tryptophanamide experiments were inconclusive in that regard. Likewise, neither set of experiments adequately displayed the inverse relationship

between pH and redox potential that prior studies had shown to occur over the entire range of pH values; instead, the effect only appeared in the middle pH values, and to a diminished extent before disappearing altogether at higher pH values. It can be said, however, that the L-Tryptophan data is largely in keeping with the hypothesis investigated in this thesis and therefore proved to be fairly valuable and insightful even if the published data it was based on was not perfectly replicated.

Although the tryptophan data support the original hypothesis (31), the data on N-acetyl-N-tryptophanamide are yet a reason for concern about the applied methodology. Future experiments will have to compare the two molecules and the two different voltammetric techniques in more depth, examine the possibility of using different electrochemical techniques and the effect, if any, of doing so on the data provided in this thesis, and certainly attempt to better replicate the results to which the results of this thesis were compared and largely based upon.

Bibliography

1. Stehle, J.; Foulkes, N.; Molina, C.; Simonneaux, P.; Pevet, P.; Sassone-Corsi P. *Nature* **1993**, 365, 314-320.
2. Molina, C.; Foulkes, N.; Lalli, E.; Sassone-Corsi, P. *Cell* **1993**, 75, 875-886
3. Alber, T. *Curr. Op. Gen. & Dev.* **1992**, 2 (2), 205-210.
4. Landschulz, W.; Johnson, P.; McKnight, S. *Science* **1988**, 240 (4860), 1759-1764
5. Ellenberger, T. *Curr. Op. Struc. Bio.*, **1994**, 4 (1), 12-21.
6. Sessa, G.; Morelli, G.; Ruberti, I. *J. Mol. Bio.*, **1997**, 274 (3), 303-309.
7. Gelin, B.; Lee, A.; Karplus, M. *J. Mo. Bio.* **1983**, 171 (4), 489-559.
8. Jung, K.; Rhee, H.; Park, C.; Yang, C. *Biochim. Biophys. Res Commun* **2005**, 334 (1), 269-275.
9. Rishi, V.; Potter, T.; Laudeman, J.; Reinhart, R.; Silvers, T.; Selby, M.; Stevenson, T.; Krosky, P.; Stephen, A.G.; Acharya, A.; Moll, J.; Oh, W.-J.; Scudiero, D.; Shoemaker, R. H.; Vinson, C. *Anal. Biochem.* **2005**, 340, 259-271.
10. Fedorova, A.V.; Chan, I.-S.; Shin, J.A. *Biochim. Biophys. Acta* **2006**, 1764, 1252-1259.
11. Chan, I.-S.; Fedorova, A.V.; Shin, J.A. *Biochemistry* **2007**, 46, 1663-1671.
12. Dragan, A.I.; Frank, L.; Liu, Y.; Makeyeva, E.N.; Crane-Robinson, C.; Privalov, P.L. *J. Mol. Biol.* **2004**, 343, 865-878.
13. Palena C.; Tron, A.; Bertoncini, C.; Gonzalez, D.; Chan, R. *J. Mol. Bio.* **2001**, 308 (1), 39-47.
14. Diebold, R.J.; Rajaram, N.; Leonard, D.A.; Kerppola, T.K. *Proc. Natl. Acad. Sci.* **1998**, 95, 7915-7920.
15. Ellenberger, T.; Brandl, C.; Struhl, K.; Harrison, S. *Cell* **1992**, 71 (7), 1223-1237.
16. Smith, P.K.; Krohn, R.; Hermanson, G.; Mallia, A.; Gartner, F.; Provenzano, M.; Fujimoto, E.; Goeke, N.; Olson, B.; Klenk, D. *Anal. Biochem.* **1985**, 150 (1), 76-85
17. Brown, R.; Jarvis, K.; Hyland, K. *Anal. Biochem.* **1989**, 180 (1), 136-139.
18. Clegg. *Curr. Op. Biotech.* **1995**, 6, 103-110.
19. Stryer, L.; Haugland, R. *Proc. Nat. Acad. Sci.* **1967**, 58 (2), 575-578.

20. Breunig, M.; Lungwitz, U.; Liebl, R.; Goeferich, A. *Eur. Jour. Pharm. Biopharm.* **2006**, 63 (2), 156-165.
21. Federova, A.; Chan, I.; Shin, J. *Biochemistry* **2007**, 46 (6), 1663-1671.
22. Sancar, A. *Chem Rev.* **2003**, 103, 2203-2237.
23. Lipkin, R. *Science News.* **1995**, 148 (2), 20.
24. Hagmann, M. *Science Now*, **2000**, 3, 1.
25. Zoltowski, B.; Vaidya, A.; Top, D.; Widom, J.; Young, M.; Crane, B. *Nature*, **2011**, 480, (7377), 396-399.
26. Kulms, D.; Poppelmann, B.; Yarosh, D.; Luger, T.; Krutmann, J.; Schwarz, T. *PNAS* **1999**, 96 (14), 7974-7979.
27. Li, Y. F.; Heelis, P. F.; Sancar, A. *Biochemistry* **1991**, 30, 6322-6329.
28. Aubert, C.; Vos, M. H.; Mathis, P.; Eker, A. P. M.; Brettel, K. *Nature* **2000**, 405, 586-590.
29. Byrdin, M.; Lukacs, A.; Thiagarajan, V.; Eker, A.P.M.; Brettel, K.; Vos, M.H. *J. Phys. Chem.* **2010**, 114, 3207-3214.
30. Byrdin, M.; Sartor, V.; Eker, A. P. M.; Vos, M. H.; Aubert, C.; Brettel, K.; Mathis P. *Biochim. Biophys. Acta* **2004**, 1655, 64-70.
31. Zieba, A.; Richardson, C.; Lucero, C.; Dieng, S.; Gindt, Y.; Schelvis, J. *J. Am. Chem. Soc.*, **2011**, 133 (20), 7824-7836.
32. Sjödin, M.; Styring, S.; Akermark, B.; Sun, L.; Hammarström, L. *J. Am. Chem. Soc.* **2000**, 122, 3932-3936.
33. Sjödin, M.; Ghanem, R.; Polivka, T.; Pan, J.; Styring, S.; Sun, L.; Sundström, V.; Hammarström, L. *Phys. Chem. Chem. Phys* **2004**, 6, 4851-4858.
34. Sjödin, M.; Styring, S.; Wolpher, H.; Xu, Y.; Sun, L.; Hammarström, L. *J. Am. Chem. Soc.* **2005**, 127, 3855-3863.
35. Marcus, R. A.; Sutin, N. *Biochim. Biophys. Acta* **1985**, 811, 265-322.
36. Kapetanaki, S. M.; Ramsey, M.; Gindt, Y. M.; Schelvis, J. P. M. *J. Am. Chem. Soc.* **2004**, 126, 6214-6215.
37. Chang, T.K.; Chaing, Y.; Guo, H.; Kresge, A.; Mathew, L.; Powell, M.; Wells, J. *J. A. Chem. Soc.* **1996**, 188, 8802-8807.
38. Wiberg, K.; Slauch, L.; *J. Am. Chem. Soc.* **1958**, 80, 3033.

39. Schowen, K.B.; Schowen, R.L. *Meth. Enzym.* **1982**, 87, 551-606.
40. Lopez, M. M.; Makhatadze, G. I. *Biophys. Chem.* **1998**, 74, 117-125.
41. Cleland, W. W. *J. Bio. Chem.* **2003**, 278 (52), 51975-51984.
42. Dr. Carlstein Biele. Fiz Chemie Berlin – Kinetic Isotope Effect.
http://www.chemgapedia.de/vsengine/vlu/vsc/en/ch/12/oc/vlu_organik/aufklaerung/aufklaerung_d_isotopeneffekte.vlu/Page/vsc/en/ch/12/oc/aufklaerung/a9_isotopeneffekte1/a9_isotopeneffekte1.vscml.html (accessed 4/3/12).
43. IUPAC. Compendium of Chemical Terminology, 2nd ed. (the "Gold Book").
Compiled by A. D. McNaught and A. Wilkinson. M. Nic, J. Jirat, B. Kosata; updates compiled by A. Jenkins. Blackwell Scientific Publications, Oxford. 1997. XML on-line corrected version: <http://goldbook.iupac.org> (2006) (accessed 4/3/12).
44. Tommos, C.; Skalicky, J. J.; Pilloud, D. L.; Wand, A. J.; Dutton, P. L. *Biochemistry* **1999**, 38, 9495-9507.
45. Zoski, C. *Handbook of Electrochemistry*. 2nd Ed. Elsevier, Boston, MA. 2007, 641.
46. Nicholson, R.S. *Anal. Chem.*, **1965**, 37 (11), 1351-1355.
47. Marcus, R. A. *Rev. Mod. Phys.* **1993**, 65 (3), 599-610.
48. Bioanalytical Systems Inc. Pulse Voltammetric Techniques.
http://www.basinc.com/mans/EC_epsilon/Techniques/Pulse/pulse.html
(accessed 4/24/12).
49. Zhao, X.; Zhang, M.; Long, Y.; Ding, Z. *Can. Jour. Chem.* **2010**, 88 (6), 569-576.
50. E. Gail, S. Gos, Rupprecht Kulzer, J. L ö rsch, A. Rubo, M. Sauer. *Cyano Compounds, Inorganic in Ullmann's Encyclopedia of Industrial Chemistry*. Wiley-VCH, Weinheim, Germany. 2007.
51. Glasoe, P.; Long, F.A. *J. Phys. Chem.* **1960**, 64, 188-189.
52. BINAS. *Informatieboek VWO-HAVO voor het onderwijs in de natuurwetenschappen*. Wolters-Noordhoff, Groningen, 1977, 100-101.
53. Harriman, A. J. *J. Phys. Chem.* **1987**, 91, 6102-6104.
54. McDougall, A. O.; Long, F. A. *J. Phys. Chem.* **1962**, 66, 429-433.
55. Paabo, M.; Bates, R. G. *J. Phys. Chem.* **1969**, 73, 3014-3017.
56. Robinson, R. A.; Paabo, M.; Bates, R. G. *J. Res. Nat. Bur. Stand. A: Phys. Chem.* **1969**, 73, 299-308.